SDC-91-120

SDC
SOLENOIDAL DETECTOR NOTES

REPORT OF THE TASK FORCE ON IMPACT OF MATERIAL IN TRACKING VOLUME

September 1991

D. Adams, P. Bonamy, J. Chapman, G. Hanson, C. Hearty, J. Hauptman, B. Hubbard, R. Hubbard, J. Hylen, W. Lockman, J.A.J. Matthews, R. Rusack, Y. Unno, B. Wicklund, Z. Wu

Report of the Task Force on Impact of Material in Tracking Volume

D. Adams, P. Bonamy, J. Chapman, G. Hanson, C. Hearty,
J. Hauptman, B. Hubbard, R. Hubbard, J. Hylen, W. Lockman,
J.A.J. Matthews, R. Rusack, Y. Unno, B. Wicklund, Z. Wu

September 1991

I. Executive Summary

The most significant impact of the material in the SDC tracking system is through e bremsstrahlung. Bremsstrahlung has the effect of smearing the e trigger threshold(s), and reduces the efficiency for identifying electrons cleanly. The limitation of the material is most stringent for the tracking elements closest to the beam. Thus it is recommended that the material in the silicon tracker is not more than 5 - 6% X_0 at $\eta = 0$, and every effort should be made to keep below this level. The restrictions on the material in the outer tracker are less stringent. However a 5 - 6% X_0 material budget is recommended to minimize the impact on the tracking trigger, and due to the significant "$1/\sin(\theta)$ effects" for the long cylindrical outer tracking system. Every effort should also be made to minimize this material, and to locate the readout ends of the outer tracker immediately adjacent to the calorimeters.

The individual results found in the report include:

1. The rates for isolated electrons from the conversion of QCD prompt photons are tolerable, relative to W$\rightarrow e^{+-}$, Top$\rightarrow e^{+-}$ etc., with 10% X_0 effective radiator before the Level 1 tracking trigger elements.

2. $\sim$ 10% X_0 of material, exclusive of internal bremsstrahlung, before the Level 1 tracking trigger elements results in a significant "softening" of the e high p_t trigger. Efforts should be made to keep below this amount of material. At this level of material, multiple scattering in the tracking system is not an issue for the trigger.

3. The material in the tracking system increases the occupancy in the outer tracking straw tubes; the level of increase is modest and considered acceptable.

4. Electron tagging requires a number of selections (cuts) that electrons must pass with high efficiency:

   - **Track Reconstruction:** Using only the silicon subsystem, with $\sim$ 6.8% X_0 at $\eta = 0$, the efficiency for reconstructing (isolated) single tracks was 98 - 99% for electrons and for muons.
   - **E/p:** With material distributed throughout the SDC tracking volume, highest E/p efficiencies are obtained using only the inner tracking system for the momentum measurement. E/p efficiencies $\sim$ 95% for $E/p < 1.5$ were obtained for a silicon system with 6.8% X_0 at $\eta = 0$.
   - **EM isolation:** The e efficiency is reduced at low $p_t \sim 10$ GeV/c, and results from bremsstrahlung occurring at or near the beam (i.e. far from the EM calorimeter). Scaling the $\sim$ 3% X_0 from internal bremsstrahlung and from material in the beam pipe to the mean radius of the silicon

tracking system, suggests that the material in the silicon tracker should not be greater than $\sim 5\%\ X_0$.

- **Track - Shower Match:** For a tracking system with $\sim 11.5\%\ X_0$ at $\eta = 0$, approximately 94% of the electrons pass a "tight" track - shower maximum $r\phi - z$ match with a rectangular window of 10 mm in the bend plane and 5 mm in the non-bend plane.

5. The material in the tracking volume does not seriously impair the calibration of the calorimeter using $Z \rightarrow e^+e^-$ events. The amount of material preceding each calorimeter tower must be known to within 5% X_0 to establish the correct peak value of E/p. The number of electrons required increases exponentially with the amount of material, and was $\sim$ 1 month at the SSC design luminosity for $\sim 16\%\ X_0$ in the tracking system.

II. Overview of Material Issues

The SDC tracking system differs in at least two significant ways from previous tracking systems in collider experiments: the tracking technologies that are matched to SSC physics have intrinsically more mass, and the desire to provide tracking over the rapidity interval $|\eta| < 2.5$ means that much of the mechanical support material for the tracking system is inside the tracker. As the SDC tracking system will have more material than previous collider experiments, it is critical to understand how this material impacts our physics capabilities. The goals of the study are to set limits on the total material in the tracking system, and to provide guidance for the design/optimization of the SDC tracking system.

The material in the tracking system directly impacts a number of triggering, efficiency and thus physics issues. Issues addressed in the report include the following:

1. **Tracking:** The issues here include how material in the tracking system influences our ability to trigger on high p_t tracks, to reconstruct tracks with high efficiency, and to measure the track momentum with precision.

   (a) *Triggering:* The material in the tracking system will result in electron bremsstrahlung and production of electron backgrounds from photon conversions. Electron bremsstrahlung will put some high p_t electrons below the tracking trigger threshold resulting in a smearing of the p_t threshold. Photon conversions will result in a number of high p_t electrons that will pass the Level 1 trigger. (Note: the most effective way to suppress the electron rate from pairs (not at Level 1) may be to have dE/dx information from the two innermost layers of the silicon tracker as used in UA2 [1].)

   (b) *Track reconstruction:* Material in the tracking system will increase the occupancies in the tracking detectors, and electron bremsstrahlung may decrease the tracking efficiency for electrons.

   (c) *Momentum resolution:* Material in the tracking system degrades the resolution at low p_t as a result of multiple scattering. With the limited amount of material that can be tolerated by other consideration, this is not a critical issue [2].

2. **Calorimetry:** The issues here include how material in the tracking system influences our ability to trigger on high p_t electrons and photons, to identify electrons and photons with high efficiency, and to measure electron and photon energies with precision.

   (a) *Triggering:* Electron bremsstrahlung in the tracking system will result in several energy deposits in the EM calorimeter rather than one from the electron shower. This results in altered transverse shower profiles, as

measured in EM towers and in the strip detectors at shower maximum, but should have a small effect on the longitudinal EM energy profile. Photon conversions may result in a loss of prompt high p_t photons at the trigger level; at a minimum, pair conversion of these photons complicates the prompt photon and electron triggers and analyses.

(b) e/γ *ID:* Electromagnetic showers are identified by requiring that Had/EM is small, plus transverse shower profiles consistent with an EM shower. e/γ separation is achieved by identifying a charged track pointing at the EM shower. $e/\pi^{\pm}\pi^{0}$ separation is achieved by track - shower matching using the strip detectors at shower maximum, and by requiring a selection on E/p near 1. The essential demand is that the final electron sample must be clean, and this selection must be achieved with high efficiency.

3. e/γ **Energy Measurement:** The tracking material will result in some energy being lost from the calorimeter cluster energy, and will result in an altered momentum for electron tracks due to bremsstrahlung. The critical issue is to be able to calibrate the calorimeter both in real time and absolutely. Calibration of the EM calorimeter can be accomplished using $Z \rightarrow e^{+}e^{-}$ events.

The report discusses triggering issues in section III, electron ID issues in section IV, and EM calorimeter calibration in section V. Section VI provides a "target" material budget for a tracking system that is near the upper end of material consistent with the identification of electrons with high efficiency.

III. Triggering

III.1) Conversion Electrons in the SDC Central Tracker

We summarize a preliminary analysis of the rates for conversion electrons in the SDC detector, relative to other interesting sources of prompt electrons. We have used Papageno V3.30, and other available NLO calculations to estimate inclusive rates in the central region (η less than 2.0), and we have cross checked these using CDF data at 1.8 TeV [3]. We have considered three sources of "isolated" electrons, namely

(1) Inclusive W/Z production.

(2) Top quark (Mt=140).

(3) QCD prompt photon production, followed by conversion in 10% X_0. This value approximates the inner silicon detector at SDC. Additional conversions will occur in the outer tracking chamber, but the trigger and track reconstruction efficiency will be lower.

We have also considered "nonisolated" leptons coming from

(4) Inclusive Bottom production

(5) Photon conversions resulting from π^0, η production in jets.

(6) High p_t hadrons faking electrons.

The efficiency for triggering and reconstructing nonisolated electrons is detector dependent, but we can get an idea of the relative rates for these "electrons" from the CDF data. While the SDC cross sections are typically X10 higher, and harder in p_t, the relative rates for the parton level processes,

(a) W + jet(s)

(b) QCD Photon + jets

(c) b + Jet(s)

(d) $\pi^0 \rightarrow \gamma$, or fake hadron

all scale rather similarly as functions of p_t or x_t.

For process (a), the full NLO calculation [4] agrees with the CDF p_t(W,Z) distributions at 1.8 TeV; lowest order Papageno (W + 1 jet) gives an adequate description of these data, provided an overall K=2.2 factor is applied to Papageno. For process (b), we have NLO predictions [5] at 1.8 and 40 TeV, the former in fair agreement with CDF data; the NLO predictions agree with lowest order Papageno

(γ + 1 jet), using a K=3 factor. For process (c), the NLO rates [6] require a K=3 factor, compared with lowest order Papageno.

Figure 1 shows the inclusive electron rates at CDF for $\eta \leq 0.7$, 4.1 pb-1. The electron isolation cuts give an efficiency of 40-50% on the low p_t continuum, which includes bottom electrons (60%), non-identified conversions (18%), and hadron fakes (22%). The W/Z jacobean peak is evident. The total rate for identified conversions, which are removed from fig. 1, is approximately 28% of the low p_t continuum in fig. 1. Of the found conversions, we estimate that 30-35% come from QCD prompt photon production, based on their isolation properties. The remaining found conversions are presumably due to π^0, η decays in jets. The nonidentified conversions (18% of the low p_t continuum) are conversion pairs in which the partner positron has low momentum, so that the track reconstruction efficiency is low.

Figure 2 shows the predicted electron spectra at 1.8 TeV, averaged over ($\eta \leq 2$), from W decay and QCD prompt photons (we use Bethe Heitler to describe the photon conversion to electron pairs, and integrate the total electron rate with no cuts on tagging efficiency.) The solid curve for prompt photons corresponds to 10% X_0. The dashed curve is an interpolation of the rate for isolated conversion electrons seen in CDF. We have normalized the observed conversion rate to the W electron peak. The dashed curve is consistent with the solid curve prediction for prompt photons, taking into account the 4.6% X_0 equivalent radiator inside the CDF central tracker. Figure 3 shows the same rates for the SDC. Both at CDF and SDC, the prompt photon curve crosses the W$\rightarrow e^{+-}$ curve at around 25 GeV/c p_t. Also shown in fig. 3 is the lowest order T Tbar (Mt=140) rate from Papageno. We note that the photon predictions are NLO [5], as described above; the W curve at 1.8 is a NLO prediction [4] which agrees with CDF data, and the W curve at 40 TeV is Papageno with a K factor=2.2 . (We have included the Papageno W+0 jet rates with K=1.) We emphasize that the W rates do not include Z$\rightarrow e^+e^-$; to add these, multiply the W rates by 1.2.

Aside from the overall X10 rate increase at the SDC, the W$\rightarrow e^{+-}$ curves are similar at the two energies, simply because the electron p_t spectrum is dominated by the jacobean peak in the W $\rightarrow e\nu$ decay; this peak is smeared more at the higher energy, due to the harder intrinsic p_t(W) spectrum. With a "reasonable" high luminosity trigger, Et> 50, integrated over +-2 units of η, we expect around 2 Hz at 10**33 from W and Top electrons, with 40% conversion background. This may be a reasonable choice for an inclusive single electron trigger, which has been used successfully for virtually all of the heavy flavor and electroweak studies carried out at CDF (CDF used a 12 GeV Et threshold.)

To summarize, the rates for isolated electrons from the conversion of QCD prompt photons, relative to W$\rightarrow e^{+-}$, Top$\rightarrow e^{+-}$ etc., are expected to be tolerable with 10% X_0 effective radiator before the Level 1 tracking trigger elements. In particular, the isolated conversions, illustrated in figs. 2 and 3, should have similar isolation properties (except for the presence of a partner positron) as the electrons

from W and Top sources; they should give about half the W$\rightarrow e^{+-}$ rate for Et$\geq$ 50 GeV. From kinematics, we would expect the conversion finding efficiency to be high (~80%), but this needs more detailed simulation. If the conversion identification is well understood, these isolated conversions can be used as a control sample in studies of lepton plus multijet final states (as at CDF.)

The isolated conversions are only part of a low p_t continuum, which will include nonisolated conversions, bottom/charm decays, and hadron fakes. If we extrapolate these rates from CDF, assuming the same efficiencies for nonisolated electrons, we predict (Table 1) the following mix for the low p_t ($p_t \leq 20$) continuum:

Table 1: Contributions to Low p_t "Electrons"

		CDF	SDC
(1)	b,c,fakes	64%	47%
(2)	Unseen Conversions	14%	21%
(3)	Seen Conversions	22%	32%
	Total	100%	100%
(4)	Isolated Conversions	11%	16%

The precise mix depends on isolation cuts. We are assuming that the main sources (b production and π^0 decays) scale with x_t as the prompt QCD photon rate. Taking into account the softer p_t spectrum for nonisolated electrons, one would expect this low p_t continuum to extend to the Et$\geq$50 regions in figs. 2 and 3 with rates comparable to those from isolated conversions.

Figure 4 shows an estimate for the b+bbar inclusive cross section at 40 TeV, averaged over $\eta < 1.5$, based on Ref. 7. Also shown is the corresponding p_t spectrum for electrons from these b decays, assuming an average 12% b$\rightarrow$e B.R.; there is about an order of magnitude reduction due to the kinematics of b$\rightarrow$e decay (eg p_t(e) $\ll$ p_t(b)), in addition to the B.R. Using an approximate (CDF based) simulation of the effects of a Had/EM cut, where we require Had/Em<0.04 in a 0.2 X 0.2 Had/EM region, we get the lower curve for "nonisolated" electrons from b-decay. There will be additional acceptance losses associated with overlap of π^0 showers with the electron, but these are not included in this simulation. The acceptance losses associated with a nominal Had/EM cut become quite severe for p_t(e) > 20 GeV/c, due to the hadronic fragments accompanying the electron (note that the B-meson mass and the transverse size of the hadron jet are fixed.) The actual inclusive b-quark cross section at SDC may be significantly higher than the NSD calculation (CDF observes 2.4X the NSD rate). *In general the b-rates are comparable to those for conversion electrons, depending on the actual enhancement over QCD.*

III.2) Drift Chamber Occupancy

Simulation studies have been carried out using the SDC standard simulation/analysis program, SDCSIM SHELL. The studies included the material from the beam pipe, tracking detectors plus supports, and magnet coil. Simulation of minimum bias (and Higgs) events have yielded results on straw tube occupancy and pattern recognition efficiencies [8].

The occupancy results for an eight layer straw-tube system are shown in fig. 5 for the straw outer tracker with no other material, and with a full system including beam pipe, silicon, straws, and coil. Even with a full set of material within the straw system, the innermost layer has an occupancy of about 10%. Conversions from the beam pipe/silicon slightly raise the occupancy of the inner straw superlayers somewhat. The greatest increase in occupancy is in the outer superlayers of the straw system from albedo from the coil. *The conclusion is that the increase in straw tube occupancy, from material in the tracking system, is modest and is acceptable.*

III.3) Charged Track Trigger Efficiency

Simulation studies have been carried out using the SDC standard simulation/analysis program, SDCSIM SHELL. The studies include the material from the beam pipe, and tracking detectors plus supports. Simulation results are reported for charged particle trigger efficiencies using the four axial scintillating fiber superlayers [9].

The trigger algorithm first identified cluster patterns using the hit fiber distributions in the four scintillating fiber layers in each superlayer. Acceptable hit patterns pointed essentially radially as expected for high p_t tracks. Clusters in the four axial superlayers were then linked requiring that each superlayer have a cluster and that the clusters were consistent with a circular trajectory corresponding to $p_t > p_{t_{min}}$.

Trigger efficiencies have been studied for muon and for electron tracks, and for a variation in the amount of material before the scintillating fiber outer tracker. Including the contributions for internal bremsstrahlung, the beam pipe, and the correction to $\eta = 0.5$, the effective number of radiation lengths was 3.6%, 6.5%, 10.0%, 14.4% and 25.3% in the five cases studied. With a p_t threshold of 9.5 GeV/c, the trigger was observed to be fully efficient for all muon momenta greater than 10 GeV/c. *Thus multiple scattering in the tracking system is not an issue for the trigger.*

The efficiency for electrons is shown in fig. 6 for a range of material (at 90-degrees) in the silicon subsystem. The efficiency turn-on of the electron trigger is impacted by all the material in the tracking system, but particularly by the

material before the scintillating fiber superlayers. The electron trigger inefficiency in the simulations was consistent with the probability/electron track for a hard bremsstrahlung. *Based on this, the trigger efficiency will be* $> 90\%$ *for* $p_t >$. $2 \times p_{t_{min}}$ *for* $< 10\%$ *of a radiation length (exclusive of internal bremsstrahlung) before the trigger superlayers.*

IV. Electron Identification Efficiencies

Electrons will play a crucial role in many physics processes under study at SDC. It is therefore essential that the electron detection efficiency be as high as possible. As one critical example, the detection of $H \rightarrow e^-e^-e^+e^+$ depends on the electron detection efficiency to the fourth power.

The optimization of the SDC tracking system must take into account the problem of electron bremsstrahlung as the proposed SDC tracking system has more material within the tracking volume than previous comparable systems (e.g. CDF). This is due to two main factors:

- the technologies needed to meet the requirements for precision momentum measurement and robust pattern recognition at the SSC, silicon for the inner system, straw tubes or scintillating fibers for the outer, have more radiation lengths per measurement than conventional drift chambers, and
- the need to provide tracking over the rapidity interval $|\eta| < 2.5$ results in tracking system support material in the tracking volume.

Radiation of (hard) bremsstrahlung photons can affect the electron identification efficiency in several ways. Electrons may be miss-measured in the tracking system, and/or may fail isolation or other criteria in the calorimetry. The second effect occurs because bremsstrahlung photons may cause multiple clusters in the EM calorimeter, or the displacement of the centroid of the cluster in the shower-maximum detector. Thus there is expected to be a close connection between the amount of material in the tracking system and the electron identification efficiency.

In general, we can express the efficiency for detecting an electron:

$$\mathcal{E} = \mathcal{E}_{isolation}\mathcal{E}_{tracking}\mathcal{E}_{electron\ id}$$

where $\mathcal{E}_{isolation}$ is the efficiency for the electron cluster to be isolated from other calorimeter energy (process and luminosity dependent), $\mathcal{E}_{tracking}$ is the track finding efficiency for isolated tracks, and $\mathcal{E}_{electron\ id}$ is the efficiency to pass all electron cuts.

In practice significant correlations may exist between these efficiencies. Thus selections (cuts) are made sequentially with the efficiency quoted for each successive cut. As an example the e ID efficiency for $|\eta| < 1$ electrons in CDF is given in Table 2 [10]. For a high e ID efficiency the efficiency for each cut should be well above 90%.

For the purposes of this study, we would like to separate this into two parts:

$$\mathcal{E}_{electron\ id} = \mathcal{E}_{E/p\ cut}\mathcal{E}_{track\ calorimetry\ match}$$

The first term is the efficiency for the track to have measured E/p less than some value to reduce the background from QCD jets ($\pi^{\pm}\pi^0$ overlap).

Table 2: CDF selection cuts and efficiencies for electrons from $Z \rightarrow e^+e^-$ with $E_T > 20$ GeV in the $|\eta| < 1$ region of the calorimeter.

Cut Type	Cut Value	Efficiency (%)
Hadron/EM	< 0.05	96.8 ± 1.3
LSHR	< 0.2	97.8 ± 1.1
$r\phi$ match	< 1.5 cm	98.9 ± 0.8
Z match	< 2.0 cm	99.5 ± 0.5
Wire χ^2	< 10	86.5 ± 2.5
Strip χ^2	< 10	96.6 ± 1.7
E/p	< 1.5	92.5 ± 1.9
Total		77.4 ± 3.1

IV.1) Electron vs Muon Tracking Efficiency ($\mathcal{E}_{tracking}$)

As bremsstrahlung causes a track's curvature to change along its trajectory, the usual track reconstruction using the full system weighting by measurement errors is not optimal for electrons. Instead, using the inner subsystem only to fit these tracks ought to have less systematic bias and a smaller tail to the E/p distribution due to radiation. It will give a less accurate p_t measurement, but for reasonably low p_t may be appropriate to base an E/p comparison on. This is the approach taken in this study [11], largely because we do not yet have a combined track reconstruction for most of the η coverage.

The study was done with single tracks simulated within the SDC GEANT program. The system simulated consisted of a 1 mm Beryllium beam pipe of radius 4 cm, the inner silicon strip subsystem, and the outer straw tube system (though only the silicon data was used in reconstruction). Two configurations for the silicon system were used: the "descope" configuration, fig. 7a, with 8 layers between 9 and 36 cm radius and 15 forward planes on each end; and the "default (LOI)" configuration, fig. 7b, with 8 layers between 18 and 39 cm radius and 22 forward planes.

The silicon simulation includes additional material in each layer specified in the parameter file, but does not simulate in detail the support structure, cooling rings, cables, etc. By default, the material in each layer consists of (at normal incidence) 0.35% X_0 of silicon and 0.5% X_0 of additional material, amounting to 6.8% X_0 at 90°. This is somewhat more than the most recent estimate for the system of 5.5% X_0 averaged over η [12].

Single electrons and muons were generated uniformly within the range $|\eta| < 2$ at several values of p_t. The track reconstruction program used the algorithm described in ref. 13.

We compared the track quality and parameters for electrons, positrons, and

muons of both signs in the pseudo-rapidity range $|\eta| < 2$. The particles were generated from $Z = 0$ at p_t values of 5, 50, and 500 GeV/c: cases where the tracking is completely multiple scattering dominated, where the effects of multiple scattering and resolution are comparable, and where it is resolution dominated. Tracks were required to have 8 points (axial or stereo) to be fit, and the fitting algorithm could add points to tracks which were missed in the initial clustering, or delete points from tracks with poor χ^2. After the fit, tracks were required to have at least 10 hits to be used.

With these criteria, the efficiency for reconstructing the single tracks was 98 - 99%. The χ^2 distributions for the different samples were nearly identical, the only noticeable difference being a small tail at high χ^2 for the 5 GeV electrons which we attribute to bremsstrahlung. The "axial" fit parameters are systematically shifted for the low p_t electrons, This effect is shown in figs. 8a and 8b for ρ (curvature) and d_0 (impact parameter), respectively, for the LOI geometry without a beam constraint imposed.

IV.2) Material Effects on Electron E/p Efficiency ($\mathcal{E}_{E/p\ cut}$)

IV.2.2) Study I

The effect of material in the tracking volume in the SDC tracking system has been evaluated by constructing various cases with the EGS4 simulations. A major difference of the SDC tracking system from the conventional system is that the material is located at the measurement location/layer, rather than in front of the tracking system which is usually created by walls of chambers. Two types of simulations were made: bunched in front of the tracking system and scatted as it is in the tracking volume [14].

Because of definitions of E, p, and collected or scattered materials, the E/p efficiencies are often different study by study and it is difficult to understand the issue/effect. This study was intended to sort out the differences and to understand the issue consistently.

The direct consequence of the material to the electrons is the electron bremsstrahlung. One approach was to collect the materials (totally or separately for the inner and the outer systems) in front of the tracking system followed by the seemingly massless tracking volume; the other was to make a scattered material geometry using EGS or GEANT and obtain the momentum by fitting the track. The first approach can use the exiting momentum after the collected material without fitting the momentum. The second approach is more realistic compared with the first approach of collected materials.

Since it is important whether we can reproduce existing data, e.g. CDF, in which the material is almost concentrated in front of the CTC (only CTC is used to get the momentum), both approaches were simulated, collected and scattered, in the EGS4 system. In both approaches the momentum of a track was obtained

by fitting the hits of an electron track to a circle in the r-phi (x-y) plane and a straight line in the s-z plane. The highest momentum track was chosen as the original electron if it showered in the material in the tracking volume. This fitted highest momentum is the definition of p in this study.

Electron tracks were traced within the whole tracking volume and showered in the coil. The showered tracks were collected if they lie within the radius of 100mm from the extrapolated entry point of the fitted highest momentum track at the surface of the calorimeter. Note: this cone is smaller than the 150mm radius used by other studies. The calorimeter energy is smeared with an energy resolution of:

$$\frac{\sigma(E)}{E} = \frac{15\%}{\sqrt{E}} \oplus 0.5\%$$

The measured energies in the calorimeter E_{meas} was rescaled E_{cal} to give the initial energy of E_0 at the peak. This E_{cal} is used for the definition of E.

At 90 degrees, $\eta = 0$, the amount of the material is the least but electron tracks will be scattered in wide η regions. Generally the effect of material is worse for lower energy electrons. The electrons from the $W \rightarrow e^+\nu$ decay make a peak around 40 GeV and populate more in the lower energy side than the higher side. Considering these factors, I have generated positrons with the transverse energy of $E_{t_0} = 20$ GeV and at $\eta = 0.5$, thus $1/\sin(\theta) = 1.13$.

To simulate the CDF design, 3.2% X_0 aluminum was placed at r=180mm, and 9 "CTC" superlayers were placed between r=200mm to 1600mm using the locations of two outer most Si-strips, Scifi's, and Straws of the SDC LOI baseline geometry. To have comparable resolving power of BL^2, the magnetic field was reduced to 1.0 Tesla (L=1.4m) instead of 1.5Tesla (L=0.9m) of the CDF. The position resolutions of the superlayers were taken to be $\sigma_{axial} = 100$ microns and $\sigma_{stereo} = 2.0$ mm. The material included: 2.9% for internal bremsstrahlung and the beam pipe, 3.2% for other material before the CTC, and 1.4% for the material in the CTC, totaling 7.5% X_0 overall at 90 degrees.

The following cases were studied:

- **SDC-I:** *collected material of the SDC/CDF design* To see a direct comparison with the above CDF design, most of the SDC material (set to 12.8% X_0) was collected at the location of r=180mm, and the $\sigma_{axial} = 60$ microns and B = 2.0Tesla were set. In this case the material included: 2.9% for internal bremsstrahlung and the beam pipe, 12.8% for most of the material in the SDC tracking system, and 1.4% (as in the CTC) for material in the tracking volume, totaling 17.1% X_0 overall at 90 degrees.

- **SDC-IIa:** *collected material of the SDC design* Because the tracking system of the SDC can be separated naturally into the inner tracking system with the Silicon and the outer tracking with the Scifi/Straw, the materials were collected at two locations: the first layer of pixel for the Silicon system (6.8% X_0), and the first layer of Scifi for the Scifi/Straw system (8.6% X_0). A

natural reason for the splitting is the vast difference of the point resolutions and the number of hits: 15 microns and 18 points, and 60 microns and 7 points. All the elements of the tracking system were turned on.

- **SDC-IIb:** *collected material of the SDC design* Following a suggestion to use only the outer tracker for the momentum measurement as in the CDF which does not include the VTPC or the SVX, the Silicon pixel and strips were turned off in the fitting of the momentum.

- **SDC-IIc:** *collected material of the SDC design* As mentioned above the SDC inner tracking system has a superior resolution and number of hits; the Silicon system is not the vertex detector in the SDC design but a tracker for the momentum measurement. With this respect the inner tracking system is a different concept from the CDF and may be sufficient for the low-momentum track measurement. The inner tracking system was turned on and the the outer tracking system was turned off.

- **SDC-IIIa:** *scattered material of the SDC design* A bunched material in front of the measurement is always the worst. The most realistic simulation is to simulate the material as it is. A geometry for pieces of material of the layers were used in the EGS for the evaluation. All the tracking element was turned on.

- **SDC-IIIb:** *scattered material of the SDC design* A direct comparison with the SDC-IIb simulation: the inner tracking system was turned off.

- **SDC-IIIc:** *scattered material of the SDC design* A direct comparison with the SDC-IIc simulation: the outer tracking system was turned off and only the inner system was turned on.

To make a systematic comparison, two variables were selected: E/p and E_0/p. The E_0 is the energy at the origin. The E is scaled to give the peak at E_0 but has spread due to the bremsstrahlung and the calorimeter resolution; E and p have positive correlation for the energy loss by bremsstrahlung. To see the bremsstrahlung tail, the fraction of events in E/p or $E_0/p > 2.0$, > 1.5, and > 1.3 were calculated and listed. Also shown is the momentum resolution of the Gaussian peak of the studied case to indicate the quality of the tracking capability. The results are summarized in Table 3.

The rows of CDF and SDC-IIb are the same quantities calculated by A.B.Wicklund [15] (only E_0/p was listed in the ref.), and the values evaluated here are consistent with his calculations; geometry and EGS calculations are reproduced. Thus the CDF data were reproduced; indicating the EGS calculation was correct. The E/p quantity (4-9% loss) was in agreement with the CDF (5-9% loss) as long as the inner tracking system was included. However, the E_0/p quantity (12-19% loss) was bad to the CDF (8-11% loss); indicating there was a rather

Table 3: Event loss fraction in E/p and E_0/p of the SDC tracking system for $E_{t_0} = 20$ GeV and at $\eta = 0.5$

Case	E/p > 2.0	E/p > 1.5	E/p > 1.3	E_0/p > 2.0	E_0/p > 1.5	E_0/p > 1.3	$\sigma(p_t)/p_t^2$
CDF	2.5%	5.6%	8.7%	4.5%	7.9%	11.1%	0.0016
CDF*	3.3%	5.8%	8.3%	(3.3%	5.8%	8.3%)	0.002
SDC-I	0.5%	4.6%	10.4%	11.9%	18.7%	24.8%	0.0006
SDC-IIa	0.6%	3.2%	8.3%	8.1%	14.1%	19.0%	0.0004
SDC-IIb	2.8%	6.4%	12.6%	10.8%	16.8%	22.6%	0.0012
SDC-IIc	-	-	-	-	-	-	-
SDC-IIIa	0.8%	4.2%	8.1%	7.0%	12.1%	16.2%	0.0005
SDC-IIIb	3.6%	8.4%	13.8%	10.2%	15.8%	21.3%	0.0013
SDC-IIIc	0.04%	0.7%	2.3%	4.2%	6.7%	8.9%	0.0017

*measured values with CDF (ref. 15)

large tail of bremsstrahlung effect (E/p was compensated due to the correlation in E and p).

When we care about the coincidence of the tracking and the calorimetry, the E/p is the variable for care and the values are not as bad as in ref. 15: 6 - 13% instead of 16 - 23% (in this calculation). However, if we care about the momentum of the electron, the amount of the tail is the value in ref. 15.

When the material is bunched in front of the tracking system and the momentum resolution is not good, fraction of the bremsstrahlung tail is large (SDC-IIb, SDC-IIIb). A better momentum resolution does not help very much (SDC-I, SDC-IIa). The calculations of the scattered and the bunched materials (SDC-IIa and SDC-IIIa; SDC-IIb and SDC-IIIb) are rather consistent, and this means the calculation of the scattered material is correctly done. Still, scattering the material helps to reduce the bremsstrahlung tails(SDC-IIa, SDC-IIIa).

However, the vast improvement of the situation is to use only the inner tracking system for the momentum measurement as in Study II below. The momentum resolution is comparable with CDF and the E/p is improved because the material is scattered in SDC; less is in front of the tracking volume although the total material is twice that of CDF. Care must be taken for the position matching of the extrapolated tracks and the calorimeter cluster center. The matching tail will extend to the opposite side to the bremsstrahlung tail because the fitted momentum tends to be the one before the radiation (although the rms deviation is small (9mm) compared to the probable tower size of 100mm). The resulting

deviation was rather symmetric than asymmetric in which only bremsstrahlung tail exited.

To take the full advantage of the SDC tracking system, only the inner tracking system is used for low energy electrons. This provides comparable E/p efficiency to CDF and results in comparable momentum resolution for the low momentum tracks. It is a wrong idea to treat the inner tracking system as the vertex detector; it is the momentum measurement device and gives a comparable or better tracking for the low momentum tracks (and is valuable for the TeV/c muons decaying from a new gauge bosons of TeV scale).

IV.2.1) Study II

The simulation described in section IV.1 above was used to estimate the efficiency for electrons to pass various E/p selections. For this study [11], denoted Study II, the calorimeter energy E was taken to be the intial electron momentum p_{gen}. At high p_t bremsstrahlung photons will enter the EM calorimeter close to the electron and this should be a good approximation.

The distribution of $p_{gen}/p_{fit} \sim E/p$ is shown in fig. 9 for 1000 electrons with p_t=50 GeV/c and $|\eta| < 2$, comparing the cases with (solid) and without (dashes) a beam constraint imposed. The tail at high E/p is due to bremsstrahlung. The beam constraint (10μ) narrows the width the central peak, but doesn't affect the tail. This is more easily seen in the integrated plot, fig. 10, which shows the probability for an electron to be observed with $E/p < (E/p)_{cut}$. For $E/p > 1.25$, the distributions are essentially the same. These plots do not include tracking inefficiency ($\sim$ 1-2%) which was seen to be the same for electrons and muons. The E/p efficiency is the same for the descope and LOI layer configurations.

The E/p efficiency is shown for electrons of three different p_t values (10, 50 and 200 GeV/c) in fig. 11; again, for $E/p > 1.25$, the distributions are similar at the 1% level. For the remainder, we use the 50 GeV/c case. The E/p efficiency is shown for varying amounts of additional material in fig. 12, and listed in Table 4. A substantial loss is observed for moderate E/p cuts ($\sim$ 1.5) when the default material is doubled or tripled.

Although the material within the 8 layer silicon inner tracker does not introduce inefficiency for finding electrons (compared with muons) it does cause small systematic shifts and resolution tails for low p_t electrons, and introduces some inefficiency to an E/p cut. For cuts of 1.25 or greater, the E/p efficiency does not depend significantly on the track p_t, whether a beam constraint was used, or which detector configuration (LOI vs descope) is chosen. *Based on the efficiencies in Table 4, the additional material in the silicon tracking subsystem should not exceed* 0.5% X_0*/silicon layer. That is,* E/p *efficiencies* $\sim$ 95% *for* $E/p < 1.5$ *were obtained for a silicon system with* 6.8% X_0 *at* 90°.

Table 4: Single electron E/p efficiency for p_t=50 Gev/c, $|\eta| < 2$, for varying amounts of material per layer in the inner system, in addition to the 0.35% X_0 of silicon per layer.

$(E/p)_{cut}$	0.05%X_0	0.25%X_0	0.5%X_0	1.0%X_0	1.5%X_0
1.25	0.967	0.941	0.931	0.886	0.865
1.3	0.971	0.943	0.934	0.901	0.878
1.4	0.977	0.953	0.943	0.915	0.889
1.5	0.982	0.958	0.949	0.928	0.905
1.6	0.984	0.962	0.955	0.940	0.917
1.7	0.985	0.966	0.960	0.949	0.928
1.8	0.986	0.966	0.961	0.955	0.934
1.9	0.987	0.967	0.964	0.957	0.940
2.0	0.988	0.969	0.969	0.961	0.945

IV.3) EM Calorimeter Isolation Efficiency ($\mathcal{E}_{isolation}$)

To defining isolated electrons, a requirement is made that only a limited amount of electro-magnetic energy is in the EM towers adjacent to the towers containing the electron candidate. As a result of bremsstrahlung in the material of the tracking system, electrons may have a reduced efficiency to pass the EM calorimeter isolation requirement.

To study this, single electrons were generated in GEANT at 10 and 20 GeV [16]. These were aimed at the calorimeter with segmentation of 0.05 x 0.05, a mock-up of the coil, and silicon-fiber tracking system in a 2 Tesla magnetic field. The material budget was: (1) the bare silicon in the SDC LOI, (2) double the bare silicon, and (3) triple the bare silicon. Case (2) represents approximately the LOI material including supports (about 20% X_0 at 90 degrees).

The efficiency of the isolation cut was > 99% at 20 GeV and > 97% at 10 GeV. Here isolation means less than 10% of the shower energy was inside a ring surrounding the centroid of the shower in 2 x 2 0.05 x 0.05 towers; that is, more than 90% of the shower energy was inside a box 0.1 x 0.1 in $\eta - \phi$. Within the limited statistics of this study, the efficiencies were constant at the 1% level for cases (1) - (3).

To obtain a more detailed understanding of how material in the tracking volume will result in isolation cut inefficiencies it is instructive to determine the separation between a (hard) bremsstrahlung photon and the electron at the calorimeter [17]. For transverse momenta of interest, $p_t > 10$ GeV/c, the $\gamma - e$ separation depends only on the final electron transverse momentum, p_t', (following the bremsstrahlung) and on the radial position where the bremsstrahlung occurred. The size of an EM tower, 10 cm, was chosen to set the scale of $\gamma - e$ separations below which an isolation cut should be efficient. For $\gamma - e$ separations to be < 10

Table 5: Efficiency for electron to have $p_t'/p_t > Fraction$ following various numbers of radiation lengths

	Efficiency (%)				
# of			*Fraction*		
X_0	0.5	0.6	0.7	0.8	0.9
0.01	99.4	99.1	98.9	98.4	97.6
0.02	98.7	98.3	97.7	96.8	95.2
0.03	98.1	97.4	96.6	95.3	92.9
0.04	97.5	96.6	95.4	93.7	90.6
0.05	96.8	95.7	94.3	92.2	88.3
0.06	96.2	94.8	93.1	90.6	86.1
0.07	95.5	93.9	92.0	89.1	83.9
0.08	94.8	93.0	90.8	87.6	81.8
0.09	94.2	92.1	89.7	86.1	79.7
0.10	93.5	91.3	88.5	84.6	77.6
0.11	92.8	90.4	87.4	83.1	75.6
0.12	92.2	89.5	86.2	81.6	73.6
0.13	91.5	88.6	85.1	80.1	71.7
0.14	90.8	87.7	84.0	78.7	69.8
0.15	90.1	86.8	82.9	77.3	67.9
0.16	89.4	85.9	81.7	75.9	66.1
0.17	88.8	85.0	80.6	74.5	64.3
0.18	88.1	84.2	79.5	73.1	62.5
0.19	87.4	83.3	78.4	71.7	60.8
0.20	86.7	82.4	77.4	70.4	59.1

cm (at the magnet coil for simplicity), the electron must have a minimum p_t after the bremsstrahlung, p_{tmin}. This is shown in fig. 13 as a function of the radial position of the (hard) bremsstrahlung. Thus electrons must retain $\sim$ 9 GeV/c if they radiate at the innermost silicon layer, but they must only retain $\sim$ 1 GeV/c if they radiate in the middle of the outer tracker.

The fraction of electrons that have $p_t' > p_{tmin}$ depends on p_{tmin}/p_t and on the amount of material in X_0 [18]. Some representative values are given in Table 5. As many physics topics would profit from achieving high lepton efficiencies for p_t values as low as $\sim$ 10 GeV/c, relevant values of p_{tmin}/p_t are as large as 0.9 (i.e. 9 GeV/10 GeV) for bremsstrahlung occurring near the beam line. As p_{tmin}/p_t decreases with increasing p_t, inefficiencies due to large $\gamma - e$ separation at the calorimeter are largest at low p_t (10 GeV/c) and are not a significant problem for $p_t > 40$ GeV/c.

To achieve high efficiencies either the amount of material must be small, and/or values of $p_t'/p_t << 1.0$ must be acceptable. As p_t'/p_t must be greater than p_{tmin}/p_t,

the large values of p_{tmin} for bremsstrahlung at small radius, fig. 13, means that material at small radius must be kept to an absolute minimum. To set the scale, the effective number of radiation lengths from internal bremstrahlung plus the material in the beam pipe is $\sim 3\%\ X_0$. This material is essentially at 0 radius. *Scaling this to the mean radius of the silicon tracking system, suggests that the material in the silicon tracker should not be greater than* $\sim 5\%\ X_0$. For comparison, the average amount of material inside the CDF central tracker is $3-4\%$ at present, and will increase to $5-7\%$ with the addition of the new SVX vertex detector.

IV.4) Shower Maximum - Track Match Efficiency ($\mathcal{E}_{track\ calorimetry\ match}$)

Electrons can be distinguished from π^0's with accompanying particles by accurate matching of the electron track to the position of the centroid of the cluster found in the shower-maximum/preshower detector [19,20]. This cut is important in reducing the background from jets, which would become large if this cut is too loose.

To understand the effect of the tracking material on our ability to make this cut, the electron track to shower matching has been simulated and the efficiency found as a function of both the material in the tracker and the size of the cut [20]. The simulations were done using GEANT 3.14.

The geometry used in this simulation was a simplified version of the "baseline" geometry. A uniform magnetic field of 2 T out to the coil and parallel to the z axis was assumed. The different materials and their thicknesses are listed in Table 6.

The tracking was simulated with 6 silicon planes and 5 fiber planes, assumed to be 100% efficient, placed outside of a thin beam pipe. Lead was placed at the vertex to simulate the internal bremsstrahlung and the superconducting coil was represented by three aluminum plates extending from a radius of 170 cm to 205 cm. Outside of the coil was an electromagnetic calorimeter, defined to have lead sheets interspersed with 2.5 mm scintillator sheets. The thickness of each lead sheet was varied to give different depth of radiation lengths, so the 2.5 mm scintillator located behind the three layers of lead/scintillator could be made to be either a preshower detector or a shower-maximum detector. For the shower-maximum, the thickness of each lead sheet was chosen to be 1 cm to give a total depth of 6.7 radiation lengths. For the preshower, the thickness was chosen to be 0.084 cm to give a total depth of 2.5 radiation length at pseudo-rapidity $\eta = 1.0$.

The effect of the tracking material on the electron identification efficiency was studied for different overall thicknesses. This was done by multiplying the amount of material in each element of the tracker by a factor m. In this study computations were made with $m = 0.01, 0.75, 1.0, 1.5$. The thicknesses of the beam pipe and the lead sheet at the vertex were kept constant. The amount material in the tracking volume was then $(2.7\% + m \times 11.5\%)X_0$ for these calculations.

Table 6: Amount of material in the "baseline" tracking volume for the shower maximum study

Material	Radius	X_0	# of layers
Internal Brem.	0cm	2.5%	1
Beam Pipe	5cm	0.2%	1
Silicon	10-45cm	5.5%	6
Fiber	70-155cm	6.0%	5
Alum. Coil	170-205cm	103%	3
Scint +	205-209cm	2%	3
Lead (SM)	"	536%	3
Lead (PS)	"	45%	3
Shower Max.	209cm	0.5%	1
Lead	209.25cm	179%	1

In this simulation, electrons were generated at the origin for the η values of 0.0, 1.0 and 1.5. To identify those tracks which could fail to be reconstructed due to the emission of a hard bremsstrahlung photon, we reconstructed the tracks and evaluated the quality of the fit. Figure 14 shows the distribution of χ^2/DOF. In this plot a long tail can be seen corresponding to those electrons which undergo a hard bremsstrahlung. In this study those tracks with χ^2/DOF greater than 2.0 are taken to have failed reconstruction. For the amount of material in the tracker defined in Table 6 above the efficiency for electrons to pass the χ^2/DOF selection was 93% at $\eta = 0.0$ and 89% at $\eta = 1.0$.

In this simulation only tracks which passed the $\chi^2/\mathrm{DOF} < 2.0$ cut were used. For a good track, the extrapolated position at the shower-maximum/preshower detectors was compared against the position of the centroid of the energy deposited by the electron shower. Only the energy deposited within ± 15 cm of the projected track was used to calculate this centroid.

The efficiencies of this matching in the bend and non-bend planes are shown in figs. 15a and b for the shower-maximum and preshower detector. Comparing the efficiencies of this matching at the shower-max and at the preshower under the same conditions, it is obvious that the matching is superior at the shower-maximum than at the preshower. This is because the number of particles at the shower-maximum detector is greater than at the preshower detector, leading to a better determination of the centroid. Comparing these two figures it is also clear that the effect of the tracking is much more significant in the bend plane than in the non-bend plane, suggesting that different cuts should be applied for two planes. This difference arises because the bremsstrahlung radiation is generally produced tangentially to the electron track and the electron, which has a lower momentum after radiating the photon, is bent further away from its initial trajectory, while continuing on the same path in the non-bend plane.

For a cut at 5 mm, it can be seen that at $\eta = 1.0$ the track to shower matching is close to 92% efficient in the bend plane and 98% for the non-bend plane.

Finally, we studied the electron efficiency when asymmetric cuts are applied in both planes simultaneously. Figure 16 shows the efficiency at $\eta = 1.0$ for different tracking materials when a rectangular cut with dimension d in the non-bend plane and $2d$ in the bend plane is applied. Note that the values of the efficiency shown in this plot are approximately equal to the product of the efficiencies found for the two views implying that they are not correlated. For the "base line" design tracking system, when a rectangular cut of $0.5 \times 1.0\ cm^2$ is applied the electron efficiency is $\sim 94\%$.

In summary, for a tracking system with $\sim 11.5\%\ X_0$ *at* $90°$, *Table 6 above, approximately 94% of the electrons pass a "tight" track - shower maximum spacial match with a rectangular window of 10 mm in the bend plane and 5 mm in the non-bend plane.* A less stringent track - shower match requirement would increase the electron efficiency but could increase the level of backgrounds. This efficiency must be combined multiplicatively with the tracking efficiency: $\sim$ **93% at** $\eta =$ 0.0 and $\sim$ 89% at $\eta = 1.0$ in this study. Consequently, at $\eta = 1.0$, $\sim$ **16% are** rejected because of bremsstrahlung radiation in the tracking volume, with the current "baseline" tracking system thickness of 11.5% X_0. If the tracking material is reduced to three quarters of the current value then $\sim$ **13% of the the electrons** are lost at $\eta = 1$. We also discovered that efficiency for track to shower match is much higher at shower-maximum than at preshower.

IV.5) E/p Efficiencies in Multi-lepton Final States

To interpret the electron efficiency results, we need to ask how they affect particular physics measurements [11]. Multi-lepton processes such as a Higgs boson are most sensitive to the efficiency, since it enters once for each lepton. For an intermediate mass Higgs, the lepton p_t distribution is shown in fig. 17. The relevant p_t range is $10 < p_t < 200$ GeV/c, so the E/p evaluated with the silicon tracking system may be appropriate in this case.

Ideally, we would like the efficiency for the 4μ, $2e2\mu$, and $4e$ final states to all have high efficiency. Perhaps a reasonable goal is $\sim 80-90\%$ after fiducial selection cuts are made. If tight E/p and other requirements are made on each electron, as would be appropriate for inclusive electrons, this will be difficult to achieve. One would probably need to adopt asymmetric cuts, tight for one electron and loose for the second. This is done, for example, in the CDF Z analysis, in which case virtually all of the jet background is removed while the efficiency is maximized [21].

For the two electron case, if we choose two cuts with efficiencies $\mathcal{E}_1$ and $\mathcal{E}_2$ ($1 > \mathcal{E}_2 > \mathcal{E}_1 > 0$), then the pair efficiency is:

$$\mathcal{E}_{1,2} = \mathcal{E}_1^2 + 2\mathcal{E}_1(\mathcal{E}_2 - \mathcal{E}_1) = 2\mathcal{E}_1\mathcal{E}_2 - \mathcal{E}_1^2$$

Expressing $\mathcal{E}_1 = 1 - \delta_1$, and assuming the single cut efficiencies are high such that we can ignore higher order terms, one finds:

$$\mathcal{E}_{1,2} \simeq \mathcal{E}_2^2$$

which means that the efficiency is essentially that of the looser cut squared. Equivalently, you only lose both electrons if they both have a catastrophic bremsstrahlung. This result is illustrated in fig. 18, which shows the single electron E/p efficiency, that efficiency squared, and the efficiency for a tight cut at $E/p < 1.2$ for one leg. If we required $E/p < 1.5$ for each leg, we get an efficiency of 90%, whereas if we require $E/p < 1.2$ for one and $E/p < 2.5$ for the other, the efficiency is 95%.

For the four electron final state, one could impose cuts in several ways. We calculated the efficiency for imposing tight cuts on all, three, two and one of the electron legs, and also for two requiring the "good" electrons to have the same sign. In all cases, the efficiency is approximately that of the looser cut to the fourth power. As before, a symmetric cut at $E/p < 1.5$ for all four electrons introduces twice the inefficiency of a tight cut at $E/p < 1.2$ on two and a loose cut at $E/p < 2.5$ on the others.

Two caveats should be made. First, as stated above, the efficiency for the E/p cut alone isn't the relevant quantity. The overall efficiency for all electron cuts is, and since the cuts are correlated, making loose E/p cuts on some electrons means you need also to have comparable efficiency for cuts on shower isolation and profile, etc, and these would need to be asymmetric in the same way. Second, it doesn't make a lot of sense to discuss these cuts without knowing what level the backgrounds would be if the cuts were loosened. Previous Higgs studies for the LOI have assumed the non-electron backgrounds to be small, but this ought to be looked at carefully.

We see that for multi-lepton events, it is important to have asymmetric cuts if this efficiency is to be maximized.

V. EM Calorimeter Calibration

The large cross section for Z production at the SSC provides many electrons for use in a tower-by-tower calibration of the EM calorimeter [22]. Although it may be possible to perform the calibration using only the measured electron energies to reconstruct the Z mass, the simplest method will be to calibrate the calorimeter to the tracking system by using E/p. The material in the tracking volume produces bremsstrahlung, which modifies the measured electron momentum and possibly the calorimeter energy. This section quantifies the subsequent impact on detector calibration.

V.1) Simulation Description

The tracking system and other material used in the simulation are summarized in Table 7. The "internal bremsstrahlung" of the Z decay is equivalent to 2.5% X_0 and is included in the beampipe material. Several variations of this base design are considered, but the number of tracking layers and the tracking resolution is held constant in all cases.

Table 7: Material in the tracking volume for Calorimeter Study

	Radius (cm)	Tracking Layers	Thickness (X_0)
Beampipe	4–5	0	0.029
Silicon	6–41	8	0.051
Outer Tracker	68–164	7	0.086
Total		15	0.166

The two components of the E/p measurement—momentum and energy—have been handled differently. EGS has been used to track electrons and photons in the 2T solenoid field until they reach the coil. The position of the highest p_t electron is recorded at each tracking plane and the transverse momentum is extracted by a circular fit. The effects of multiple scattering and bremsstrahlung are simulated by EGS and, therefore, are included in the fit; detector resolution is included by an explicit Gaussian smearing, where $\sigma_{p_t} = 0.00015 p_t^2$ (p_t in GeV).

The energies of electrons and photons reaching the coil are smeared with a calorimeter resolution of $13\%/\sqrt{E_t}$, then distributed among the 0.05×0.05 towers using a parameterized shower generator. The assumption in this calculation is that the calorimeter includes massless gaps or is otherwise capable of correcting for energy lost in the coil; a 40 GeV electron incident on the coil is measured in the calorimeter as having 40 GeV.

Forty GeV transverse momentum electrons have been simulated for $|\eta| < 0.3$ and for all values of phi. The calorimeter material has been thinned at larger η

to ensure that all particles traverse the same material thickness. The thinning is less than 5% for $|\eta| < 0.3$. The selected p_t is typical for electrons from Z decays. bremsstrahlung effects are greater for low momentum ($\sim$ 10 GeV) tracks, but the Z rate is sufficiently high that these tracks will not be needed for calibration.

V.2) Impact on E/P

Even a perfectly calibrated detector will measure an E/p distribution with a peak greater than 1.0. The true E/p distribution is peaked at 1.0 with a high side tail from bremsstrahlung (the tracker measures only the electron p_t while the calorimeter measures both the electron and photon energies). The convolution of the true distribution with the detector resolution shifts the peak to a higher values. The size of the shift depends on the amount of bremsstrahlung, the momentum and energy resolutions, and on the cell size used to enclose the EM shower energy. This analysis uses a 0.1×0.1 cell consisting of four 0.05×0.05 towers.

Figure 19 shows the E/p distribution for the standard amount of material (case A) and for three times this amount (case C). The curves are Gaussian fits to the region [0.90,1.07]. The various cases studied are summarized in Table 8. Figure 20 shows the peak value of E/p as a function of total material thickness. Note that although the distribution of material is different in each case, the peak E/p depends approximately linearly on the amount of material. The calibration relies on knowing the correct value for the peak; the material thickness preceding a tower must, therefore, be known to within 5% X_0 to ensure a systematic calibration error of less than 0.2%. Given that the total thickness at $\eta = 0$ is 16.6% X_0, this accuracy should be achievable from blueprints.

Table 8: Description of the different cases studied.

Case	Thickness (X_0)	Description
A	0.166	Baseline
B	0.332	Twice baseline
C	0.498	Three times baseline
D	0.140	Silicon 50% thinner
E	0.123	Outer tracker 50% thinner
F	0.097	Tracker 50% thinner

V.3) EM Calorimeter Calibration

As shown in fig. 19, extra material results in a wider E/p peak containing fewer events. More luminosity is required to achieve the same statistical error on the calibration. A calibration procedure using E/p has been simulated to analyse this effect.

Forty GeV electrons are simulated using EGS and parameterized showers as described above, except that a "calibration error" (α_{cal}) is applied to each tower before the four-tower sum is performed. The value of (α_{cal}) for each tower is selected from a Gaussian distribution of mean 1 and sigma 0.02. Varying the sigma from 0. to 0.06 does not significantly change the results given below.

Electrons with measured E/p between 0.90 and 1.07 are used. Although the measurement reflects to some extent the response of four different towers, the electron is assigned to the tower with the highest energy. The correction for each tower is selected to give the correct value for the average E/p for electrons assigned to that tower. The averages for the towers are not independent, so several iterations are required to obtain a consistent set of correction factors, α_{cor}. The error in the correction is $(\alpha_{cor} - \alpha_{cal})/\alpha_{cal}$. The rms of this quantity—the calibration error—is plotted in fig. 21 as a function of the number of electrons in each tower (N_e), for cases A, B, C, and F. This is total number of electrons, not just those with $0.90 < E/p < 1.07$. The errors scale as $1/\sqrt{N_e}$.

The number of electrons per tower required to achieve a calibration error of 0.3% increases approximately exponentially with the amount of preceding material, fig. 22. The specific values are $N_e = 180, 220, 520$ and 950 for cases F, A, B and C. The expected rate of $p_t > 20$ GeV electrons from Z decays is 3000 per tower per year, with a factor of 2 uncertainty. Thus, two months is sufficient to accumulate the required data for thicknesses up to twice that in the standard $\eta = 0$ case and four months for three times (50% X_0). Electrons from W decays are produced at a rate approximately five times higher, but may be more difficult to trigger on

V.4) Summary

The material in the tracking volume does not seriously impair the calibration of the calorimeter. The amount of material preceding each tower must be known to within 5% X_0 to establish the correct peak value of E/p. The calorimeter is calibrated by ensuring that the average E/p is correct for each tower individually. *The number of electrons required increases exponentially with the amount of material, but was $\sim$ 1 month for $\sim$ 16% X_0 in the tracking system.*

VI. Model Tracking Material Budget:

It is instructive to estimate the material as a function of rapidity for a model tracking system consisting of:

- contribution from (typical) internal bremsstrahlung
- thin but realistic beam pipe
- descoped silicon inner tracking system
- axial outer tracking system (No intermediate tracking is included in these material estimates. Any intermediate tracking will increase the material for large values of pseudo-rapidity and will increase the average amount of material for $|\eta| < 2.5$.)

This simple model emphasizes the $1/\sin(\theta)$ problem of long tracking systems. The material is recorded in Table 9. It is likely that significantly less material would result in significantly reduced tracking capabilities.

The material in the tracking system is 11.5% X_0 at $\eta = 0$. The material as a function of rapidity is shown in fig. 23. The average material for $|\eta| < 2.5$ is in the range 18 - 19%, and includes the contribution from internal bremsstrahlung, from the beam pipe, and from air in the tracking volume.

Table 9: Material Model for SDC Tracking System

	Radius (cm)	$\|\eta\|$ Range	Thickness (X_0)
Internal Brem	0	all	2.5%
Beampipe	5	all	$0.2\%/\sin(\theta)$
Silicon Tracker	10 - 45	< 0.9	$5.0\%/\sin(\theta)$
	"	> 0.9	$5.0\%/\cos(\theta)$
	60	all	$0.5\%/\sin(\theta)$
Outer Tracker	70 - 165	< 1.6	$6.0\%/\sin(\theta)$
Air	5 - 165	all	$0.5\%/\sin(\theta)$
Average		< 2.5	18 - 19%

References

1. R. Ansari, et al, N.I.M. A288, 240 (1990)
2. J. Hylen, "Tracking Electrons", SDC Collaboration Meeting, August 1991
3. A. B. Wicklund, "Conversion Electrons in the SDC", September 1991.
4. P. Arnold and M. Reno, Nucl. Phys. B319, 37 (1989); P. Arnold and R. Kauffman, Phys. Lett. B349, 381 (1991)
5. P. Aurenche, R. Baier, and M. Fontannaz, Fermilab-PUB 89/226/T (1989)
6. R.K. Ellis, Nucl. Phys. B303, 607 (1988); B327, 49 (1989); B335, 260 (1990)
7. Computation courtesy of R. Meng, private communication
8. G. Hanson and F. Luehring, "Tracking Material Task Force: Other Tracking Issues", SDC Collaboration Meeting, June 1991
9. D. Adams and B. Lowery, "Simulation of a SciFi Tracking Trigger for the SDC", SDC Collaboration Meeting, August 1991
10. A. Galtieri, private communication
11. B. Hubbard and W. Lockman, "Effect of Material on Electron Tracking", September 1991
12. A.Seiden, private communication, as estimated by R.Stone
13. J.Hylen, et al., "Silicon Tracker Conceptual Design Report", SCIPP-90/24 (1990)
14. Y. Unno, "The Effect of Material in the Tracking Volume – E/p Issues", September 1991
15. A. B. Wicklund, "E/p Issues for SDC", June 1991
16. J. Hauptman, "Electron Efficiencies", September 1991
17. J.A.J. Matthews, "Electron Bremsstrahlung Issues vs the Radiation Lengths in the Tracking System", SDC Collaboration Meeting, August 1991
18. Y.-S. Tsai, Rev. Mod. Phys. 46, 815 (1974)
19. R. Hubbard, "GEANT Simulations at Saclay", SDC Collaboration Meeting, June 1991;
    P. Bonamy, "Shower Maximum System Efficiency vs Tracking System Material", SDC Collaboration Meeting, August 1991

20. Z. Wu and R. Rusack, "Electron Tracking and the Track to Shower Match in SDC", September 1991

21. M.Miller, private communication

22. C. Hearty, "Impact of Tracking Material on Electromagnetic Calorimeter Calibration", September 1991

Figure Captions

Fig. 1. Inclusive electron spectrum from CDF; dashed curve shows expected charm contribution, solid shows bottom+charm . Crosses denote electron rates with W,Z electrons subtracted.

Fig. 2. Predicted electron rates at CDF from W decay and from prompt photon conversions with 10% X0. Dashed curve shows observed CDF rate for 4.6 % X0.

Fig. 3. Same as fig. 2 for 40 TeV, including Top(M=140) contribution.

Fig. 4. Inclusive rates for bottom quark (b plus bbar) production in $\eta \leq 1.5$, and for prompt e+- from b-quark decay with no efficiency cuts (top curve) and with expected Had/Em cut (bottom curve.) Electron rates include 12% semileptonic B.R.

Fig. 5. Occupancy for an eight superlayer layer straw tube system: with straws but no other material (light line), and with full system including beam pipe, silicon, straws, and coil (heavy line).

Fig. 6. SciFi trigger efficiency for electrons with a p_t threshold of 9.5 GeV/c. The effective number of radiation lengths before the SciFi system was varied between 3.6%, 6.5%, 10.0%, 14.4% and 25.3% in the five cases studied.

Fig. 7. Two configurations simulated for the inner silicon system. a) 'Descope' (now standard) configuration. b) 'Default' (LOI) system.

Fig. 8. a) Systematic shift of $\rho = -q/r_c$ (curvature) for electrons and muons at three different p_t values. b) Systematic shift of d_0 (impact parameter) for the different data sets.

Fig. 9. Distribution of $p_{gen}/p_{fit} \sim E/p$ for 50 GeV electrons comparing fit with and without a 10μ beam constraint.

Fig. 10. Efficiency for E/p to be less than $(E/p)_{cut}$ for 50 GeV electrons.

Fig. 11. Comparison of E/p efficiency for electrons of 10, 50 and 200 GeV/c.

Fig. 12. Comparison of E/p efficiency for 50 GeV/c electrons with different amounts of additional material per layer.

Fig. 13. Minimum residual electron p_t for < 10 cm $\gamma - e$ separation at the "calorimeter" as a function of the radial location of the (hard) bremsstrahlung. Initial values of p_t are 10, 20 and 40 GeV/c.

Fig. 14. χ^2 per degree of freedom distribution

Fig. 15. a) Efficiency of finding a shower as a function of the window size in bend plane for different amount of tracking materials at $\eta = 1.0$. b) Efficiency of finding a shower as a function of the window size in non-bend plane for different amount of tracking materials at $\eta = 1.0$

Fig. 16. Efficiency of finding a shower inside of a rectangle with dimension d in the non-bend plane and $2d$ in the bend plane as a function of d for different amount of tracking materials at $\eta = 1.0$

Fig. 17. Lepton p_t distribution from Isajet for a 400 GeV/c^2 Higgs boson.

Fig. 18. E/p efficiency for a pair of electrons compared with the single electron efficiency. For the pair efficiency, two curves show the efficiency for symmetric cuts in E/p and a tight cut ($E/p < 1.2$) for one electron vs the looser E/p cut applied to the other.

Fig. 19. Observed E/p distribution for (a) the baseline tracking system at $\eta = 0$ ($0.166X_0$), and (b) three times this thickness. The curves are Gaussian fits to the region $0.90 < E/p < 1.07$. Fig. 19a and b do not correspond to the same luminosity.

Fig. 20. Peak value of E/p as a function of material thickness for the six cases listed in Table 7. The dashed line has slope $0.043/X_0$.

Fig. 21. Tower-to-tower calibration error vs number of electrons per tower. Lines are of the form $\beta/\sqrt{N_e}$. Dashed is case F (half tracker-material), $\beta = 0.040$; solid is case A (baseline), $\beta = 0.046$; dotdashed is case B (twice baseline), $\beta = 0.068$; dotted is case C (three times baseline), $\beta = 0.093$.

Fig. 22. Number of electrons required to achieve 0.3% relative calibration vs preceding material thickness. The four points correspond to cases F, A, B and C. The dashed line is $N = 116 \cdot e^{X/0.234}$.

Fig. 23. Distribution of material vs rapidity for model tracking system.

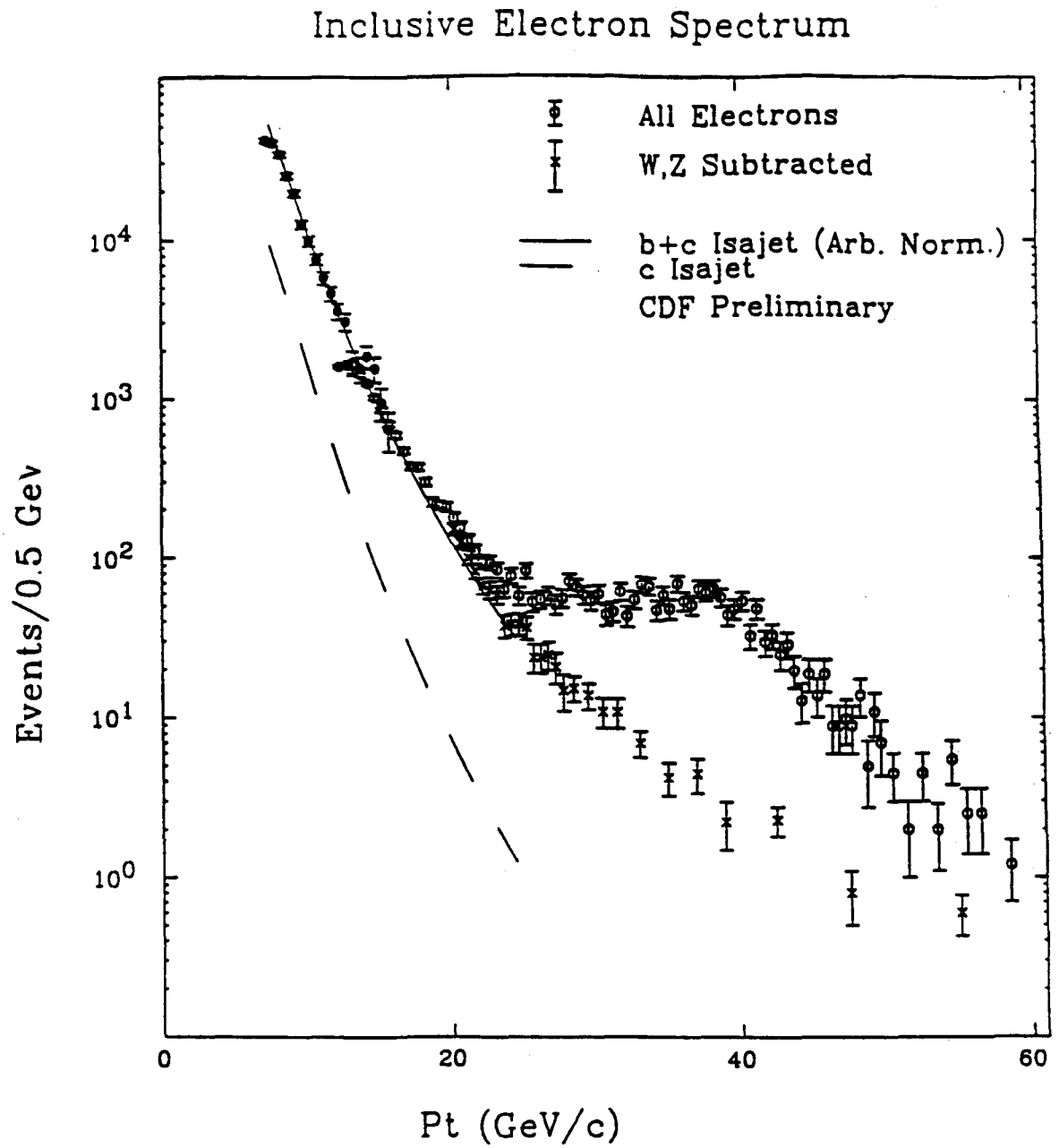
Inclusive Electron Spectrum
All Electrons
W,Z Subtracted
b+c Isajet (Arb. Norm.)
c Isajet
CDF Preliminary
Events/0.5 GeV
10^4
10^3
10^2
10^1
10^0
0
20
40
60
Pt (GeV/c)

(Fig. 1)

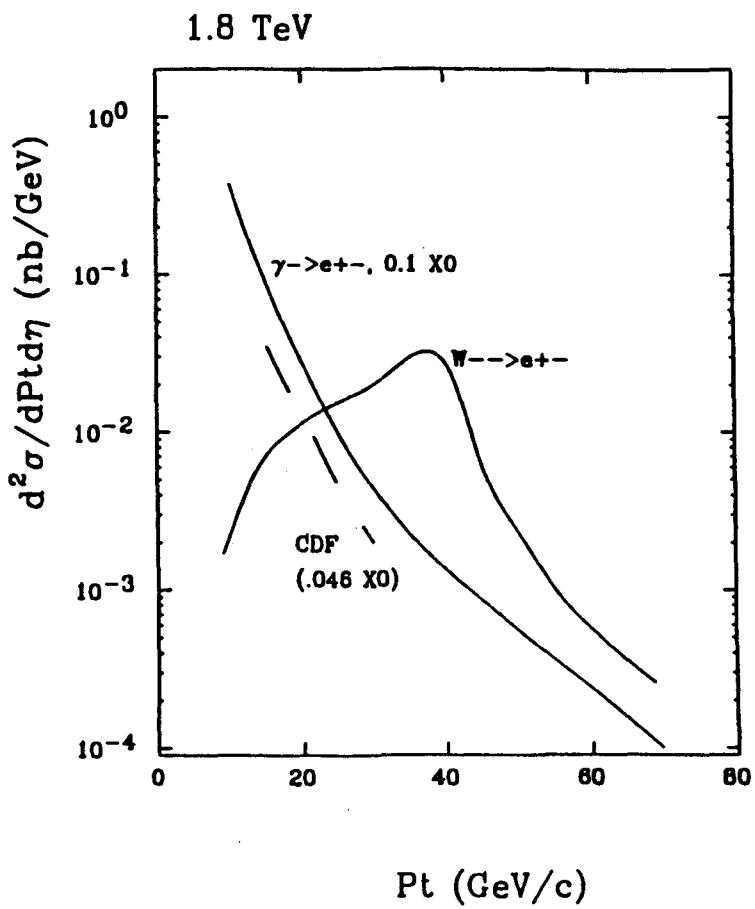
1.8 TeV
$d^2\sigma/dPtd\eta$ (nb/GeV)
10^0
10^{-1}
10^{-2}
10^{-3}
10^{-4}
γ->e+-, 0.1 X0
W-->e+-
CDF
(.046 X0)
0
20
40
60
80
Pt (GeV/c)

(Fig. 2)

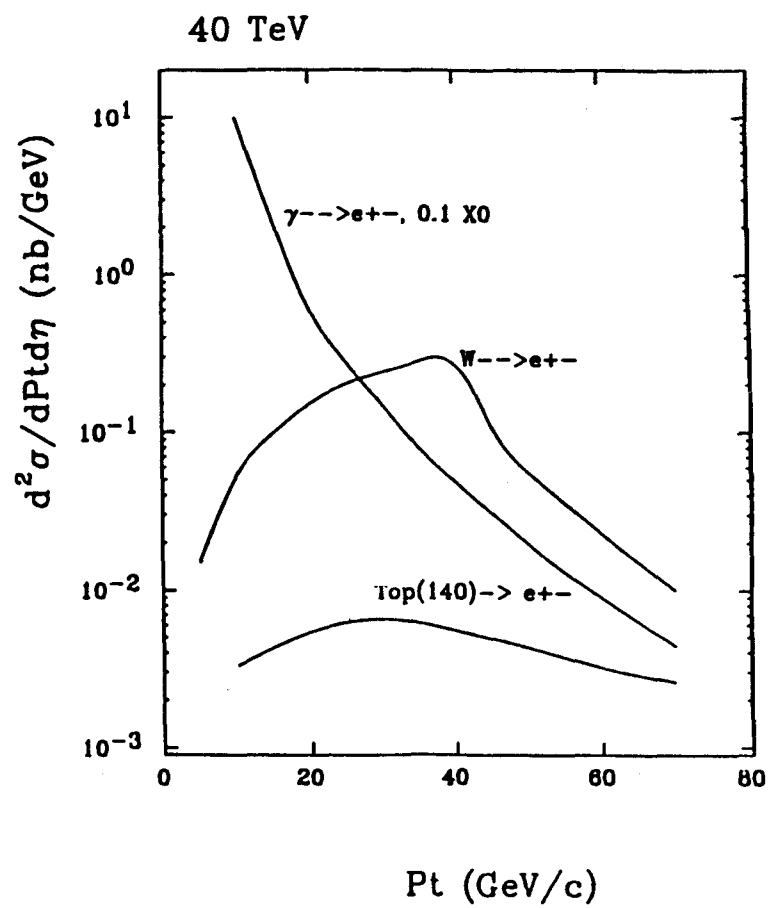
40 TeV
$d^2\sigma/dPtd\eta$ (nb/GeV)
10^1
10^0
10^{-1}
10^{-2}
10^{-3}
γ-->e+-, 0.1 X0
W-->e+-
Top(140)-> e+-
0
20
40
60
80
Pt (GeV/c)

(Fig. 3)

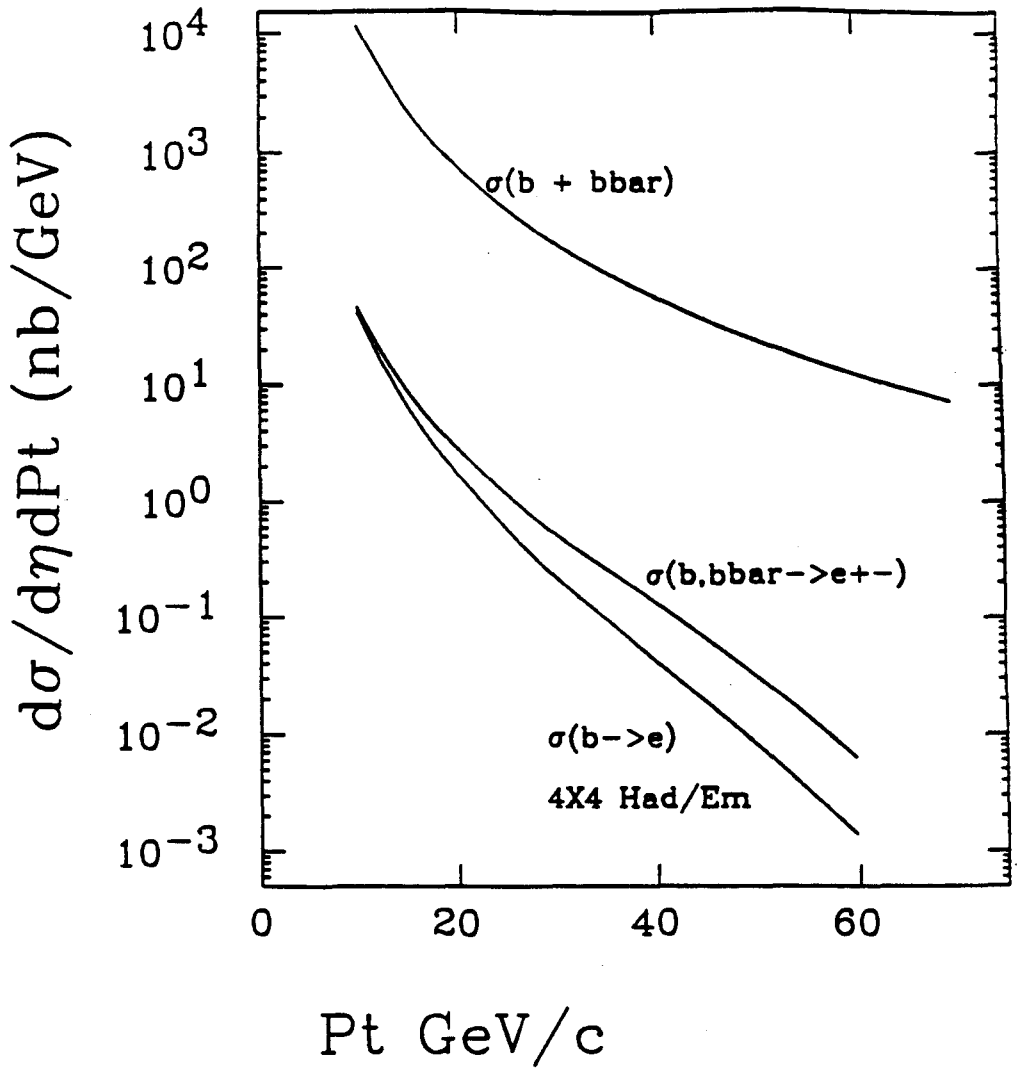
10^4
10^3
10^2
10^1
10^0
10^{-1}
10^{-2}
10^{-3}
$d\sigma/d\eta dPt$ (nb/GeV)
σ(b + bbar)
σ(b,bbar->e+-)
σ(b->e)
4X4 Had/Em
0
20
40
60
Pt GeV/c

Fig (4)

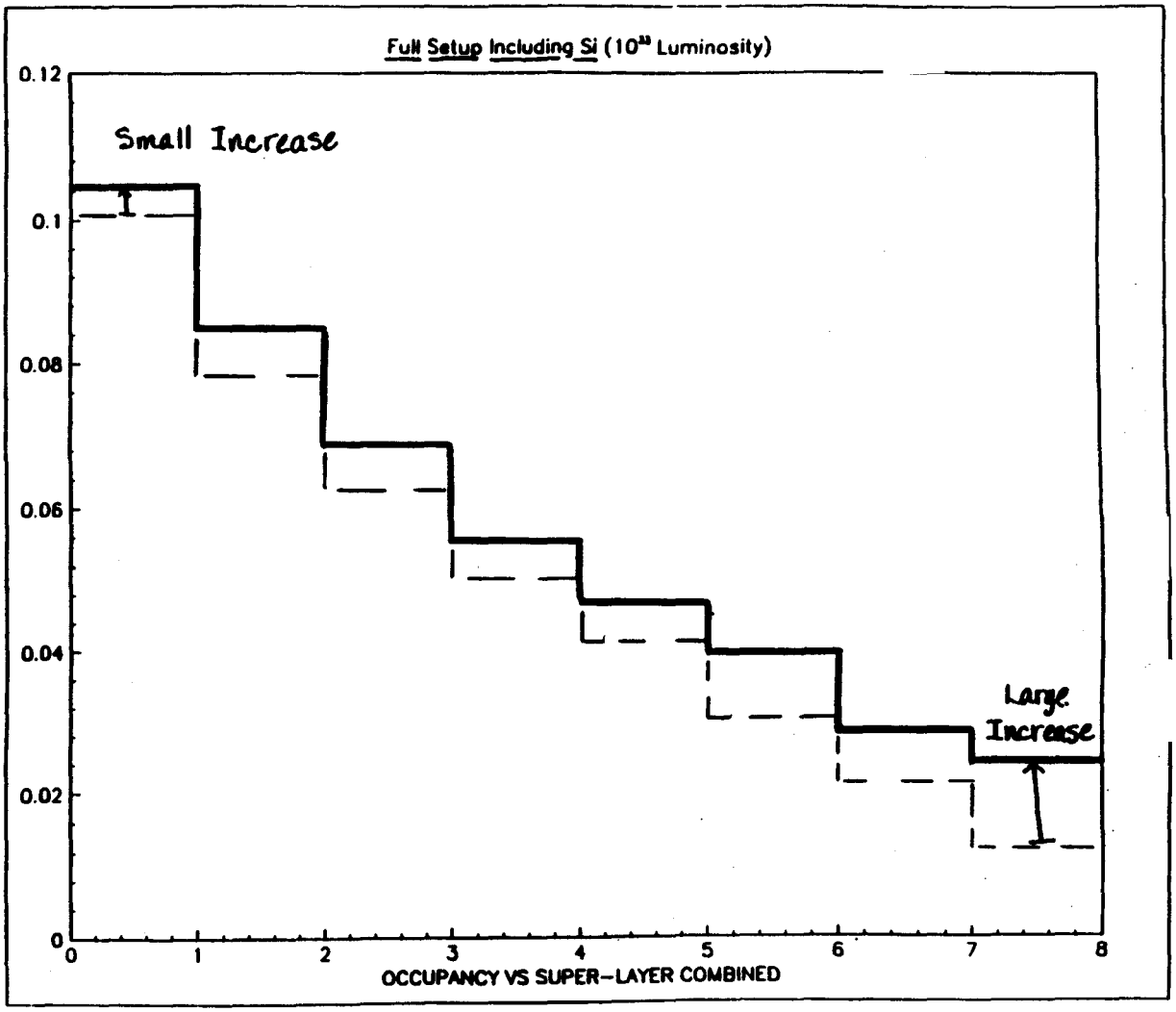

Minimum Bias Events from -20 to +4 Crossings

Fig. 5

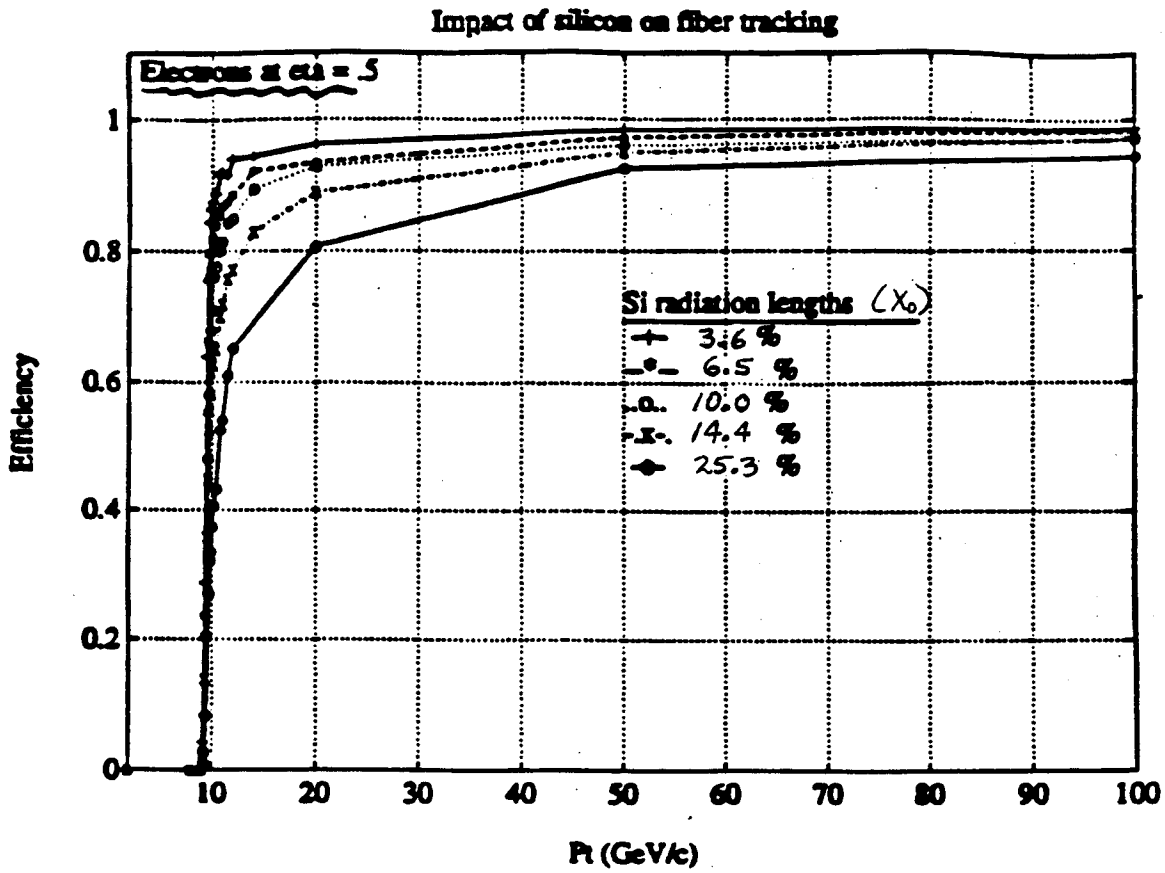
Impact of silicon on fiber tracking
Electrons at eta = 5
Efficiency
Pt (GeV/c)
Si radiation lengths (X0)
3.6 %
6.5 %
10.0 %
14.4 %
25.3 %
0
0.2
0.4
0.6
0.8
1
10
20
30
40
50
60
70
80
90
100

Fig. 6

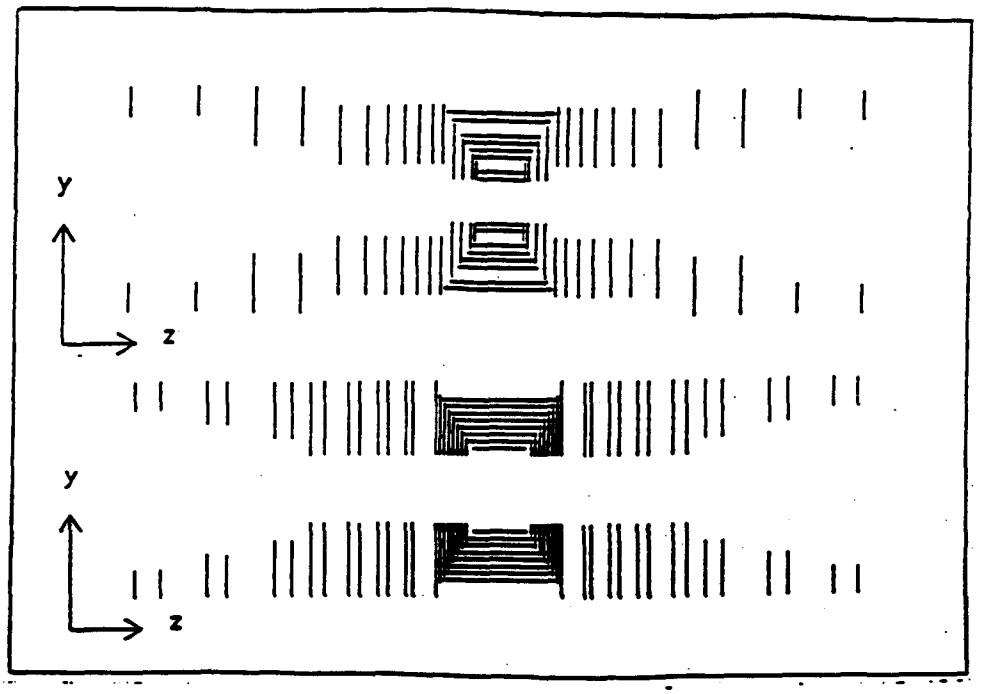

Figure 7: Two configurations simulated for the inner silicon system. A) 'Descope' (now standard) configuration. B) 'Default' (LOI) system.

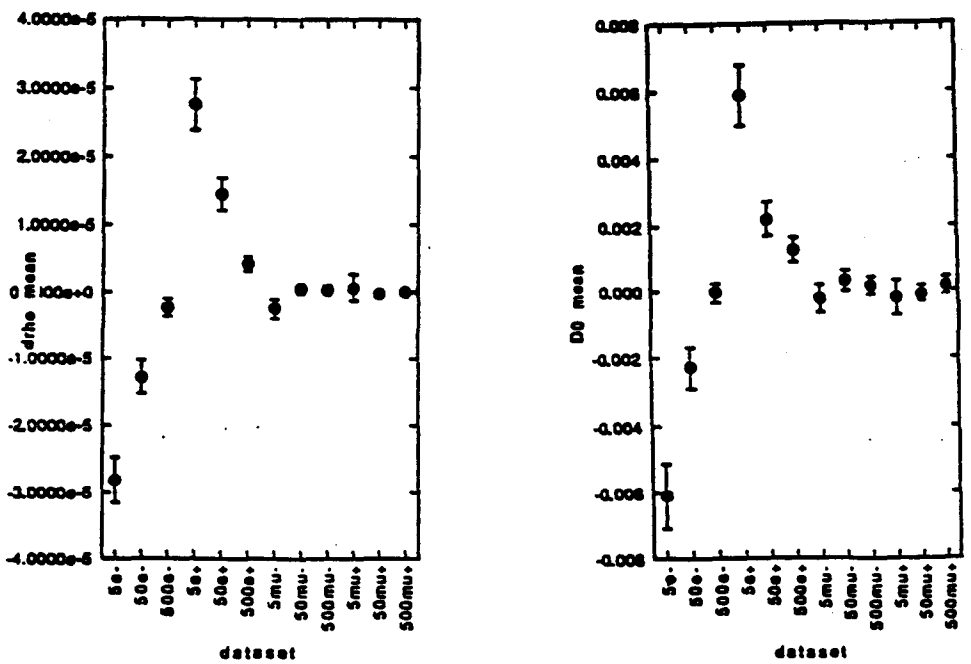

Figure 8: A) Systematic shift of $\rho = -q/r_c$ (curvature) for electrons and muons at three different p_t values. B) Systematic shift of d_0 (impact parameter) for the different data sets.

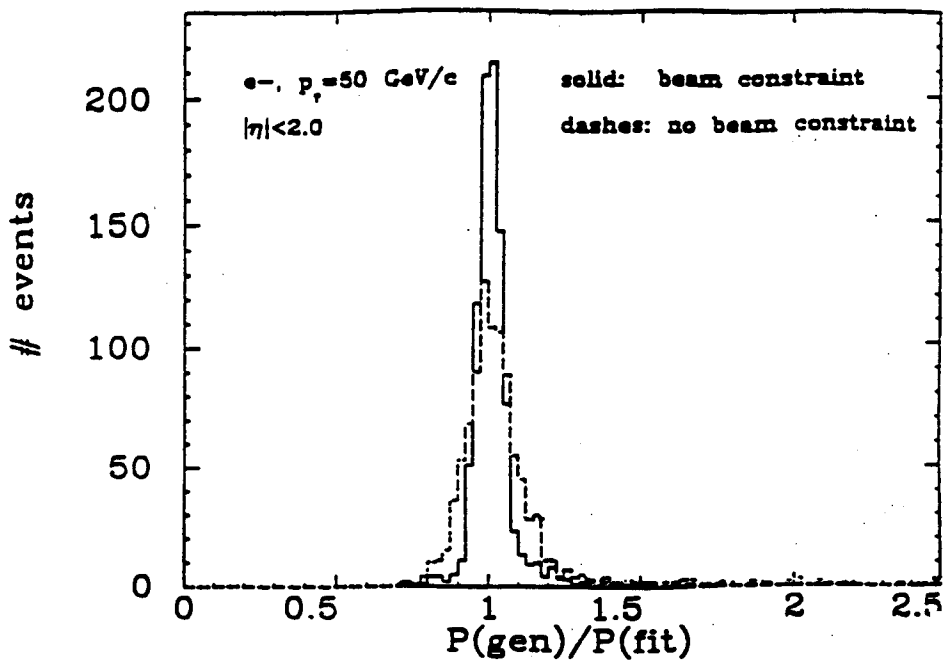

Figure 9: Distribution of $p_{gen}/p_{fit} \sim E/p$ for 50 GeV electrons comparing fit with and without a 10μ beam constraint.

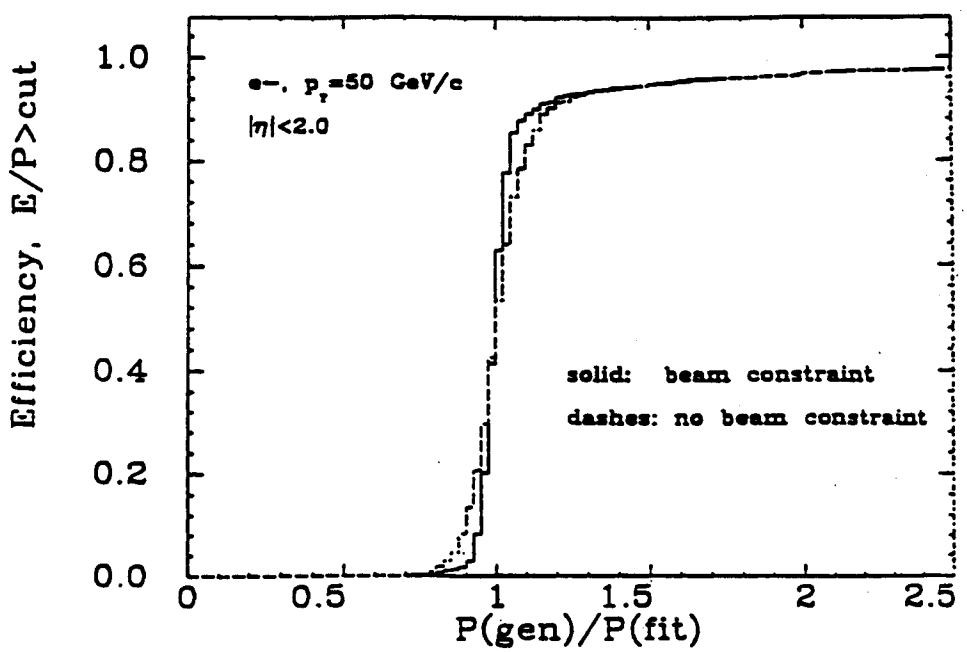

Figure 10: Efficiency for E/p to be less than $(E/p)_{cut}$ for 50 GeV electrons.

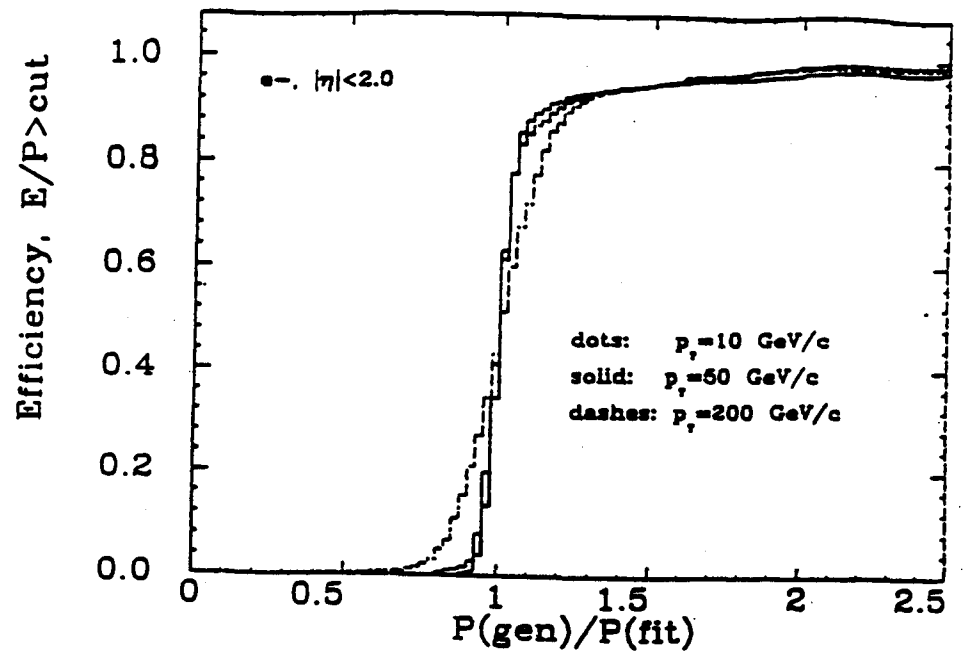

Figure 11: Comparison of E/p efficiency for electrons of 10, 50 and 200 GeV/c.

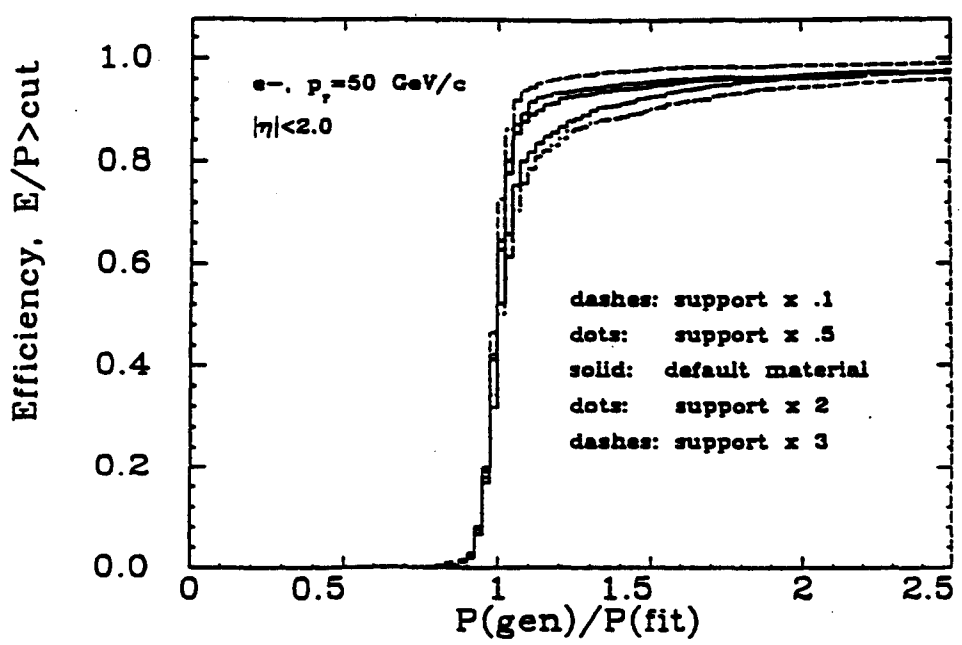

Figure 12: Comparison of E/p efficiency for 50 GeV/c electrons with different amounts of additional material per layer.

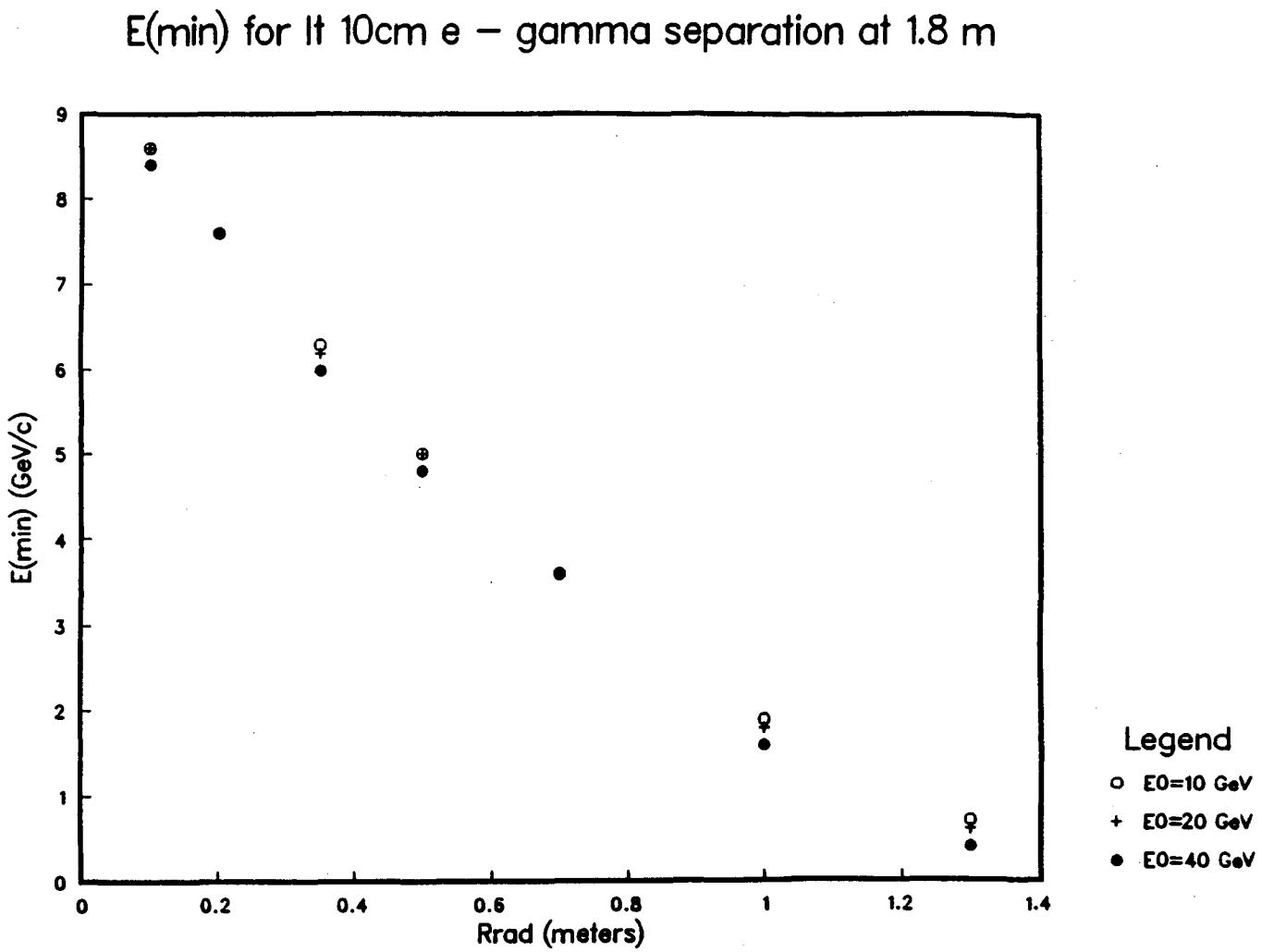
E(min) for lt 10cm e − gamma separation at 1.8 m
E(min) (GeV/c)
Rrad (meters)
0
1
2
3
4
5
6
7
8
9
0
0.2
0.4
0.6
0.8
1
1.2
1.4
Legend
E0=10 GeV
E0=20 GeV
E0=40 GeV

Fig. 13

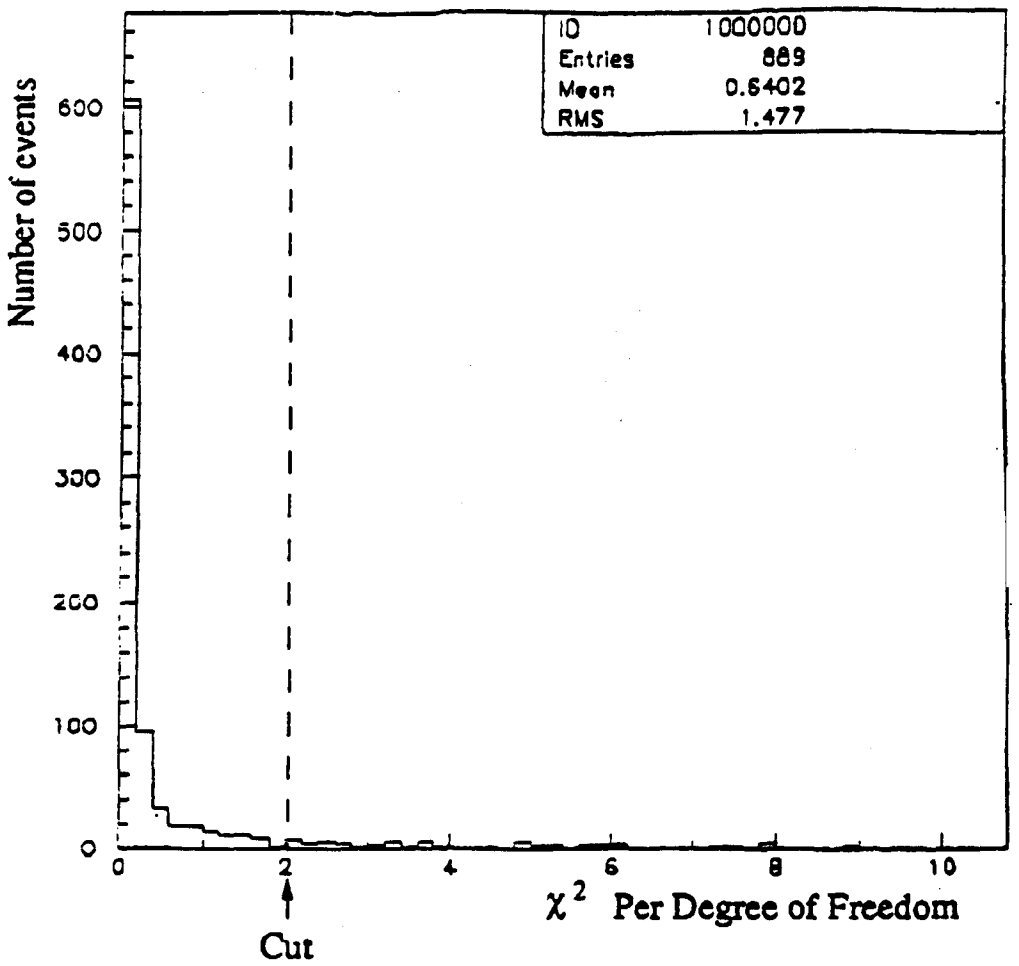

Figure 14 χ^2 per degree of freedom distribution

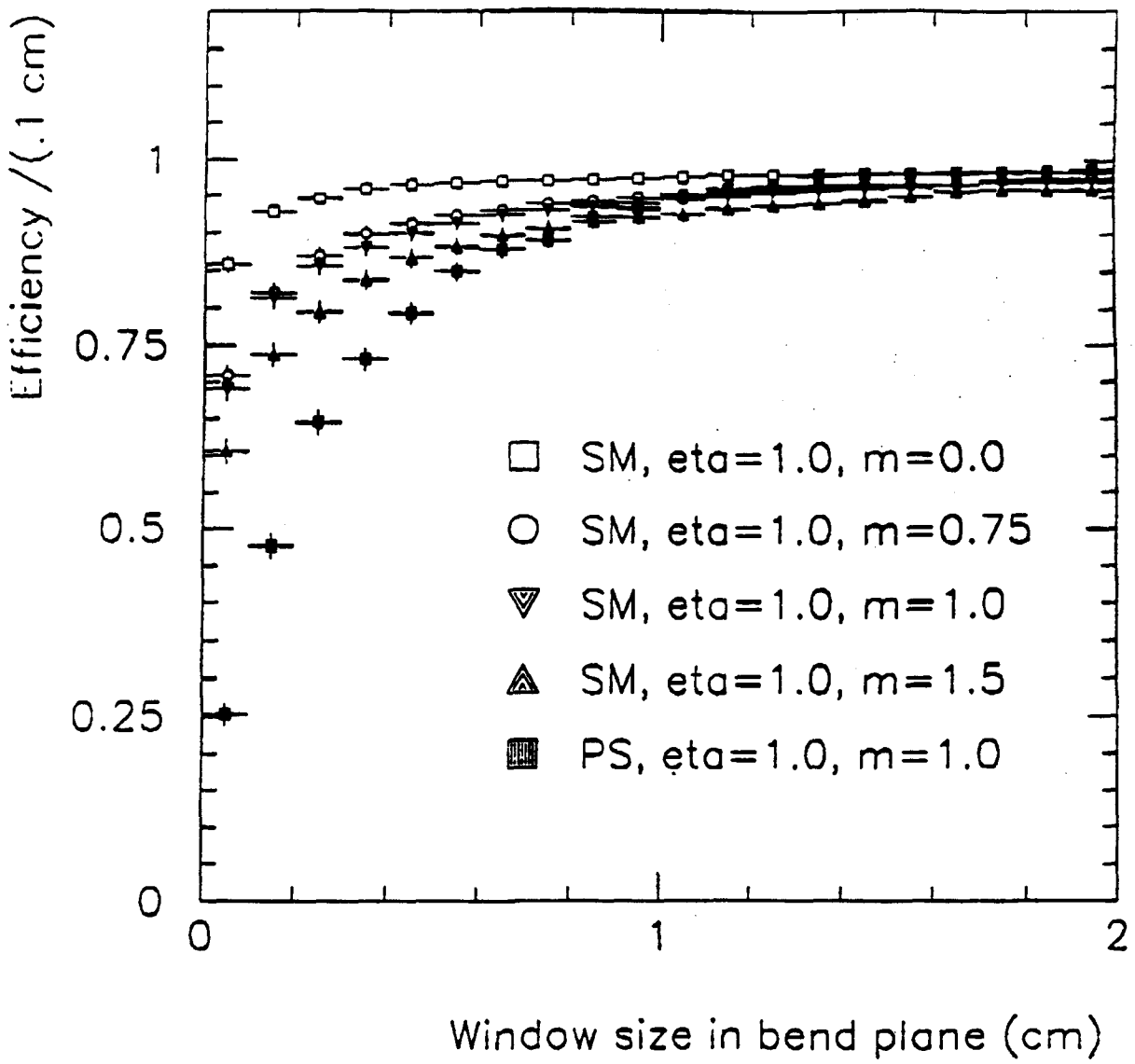

Figure 15a Efficiency of finding a shower as a function of the window size in bend plane for different amount of tracking materials at $\eta = 1.0$

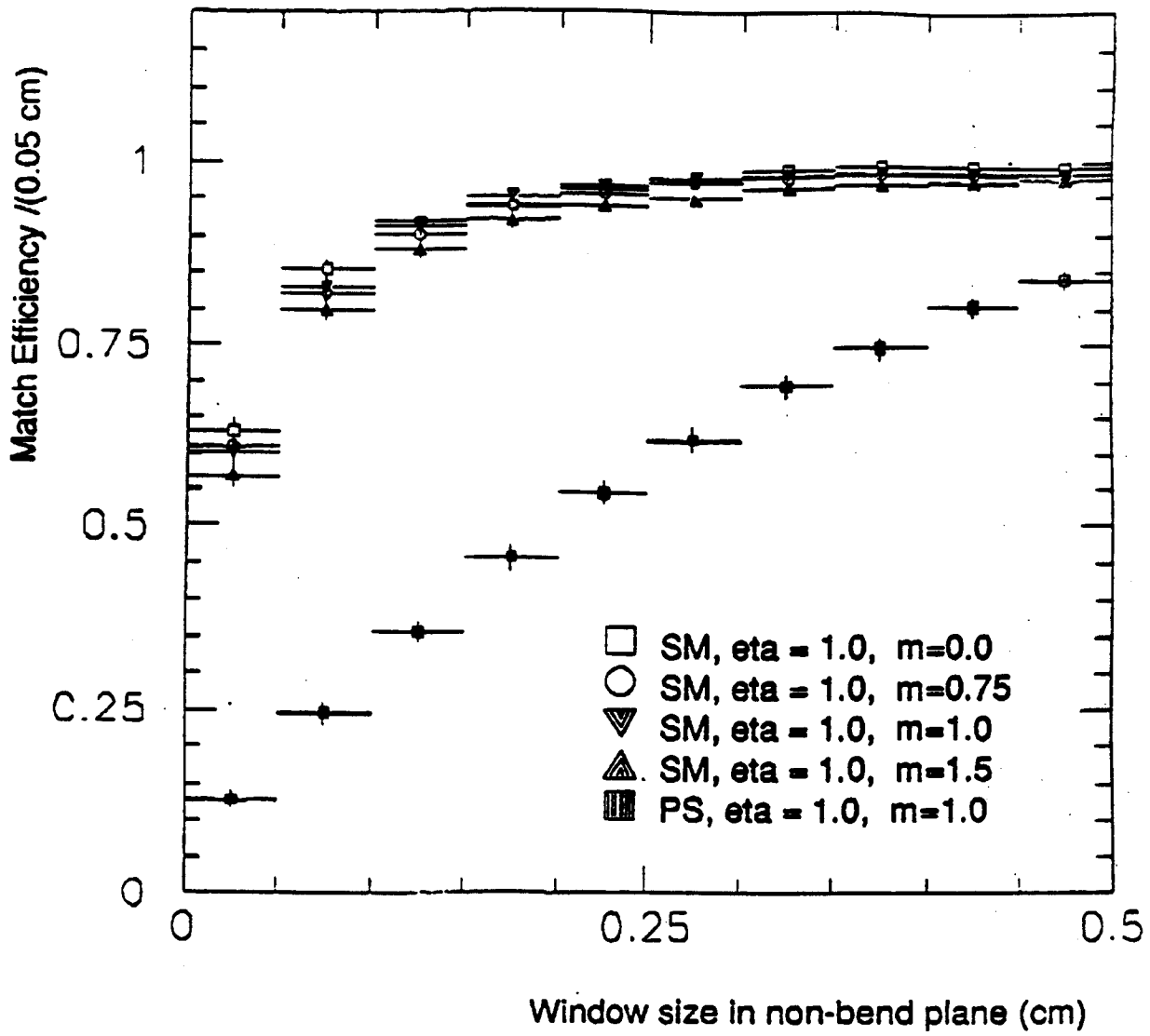

Figure 15b: Efficiency of finding a shower as a function of the window size in non-bend plane for different amount of tracking materials at $\eta = 1.0$

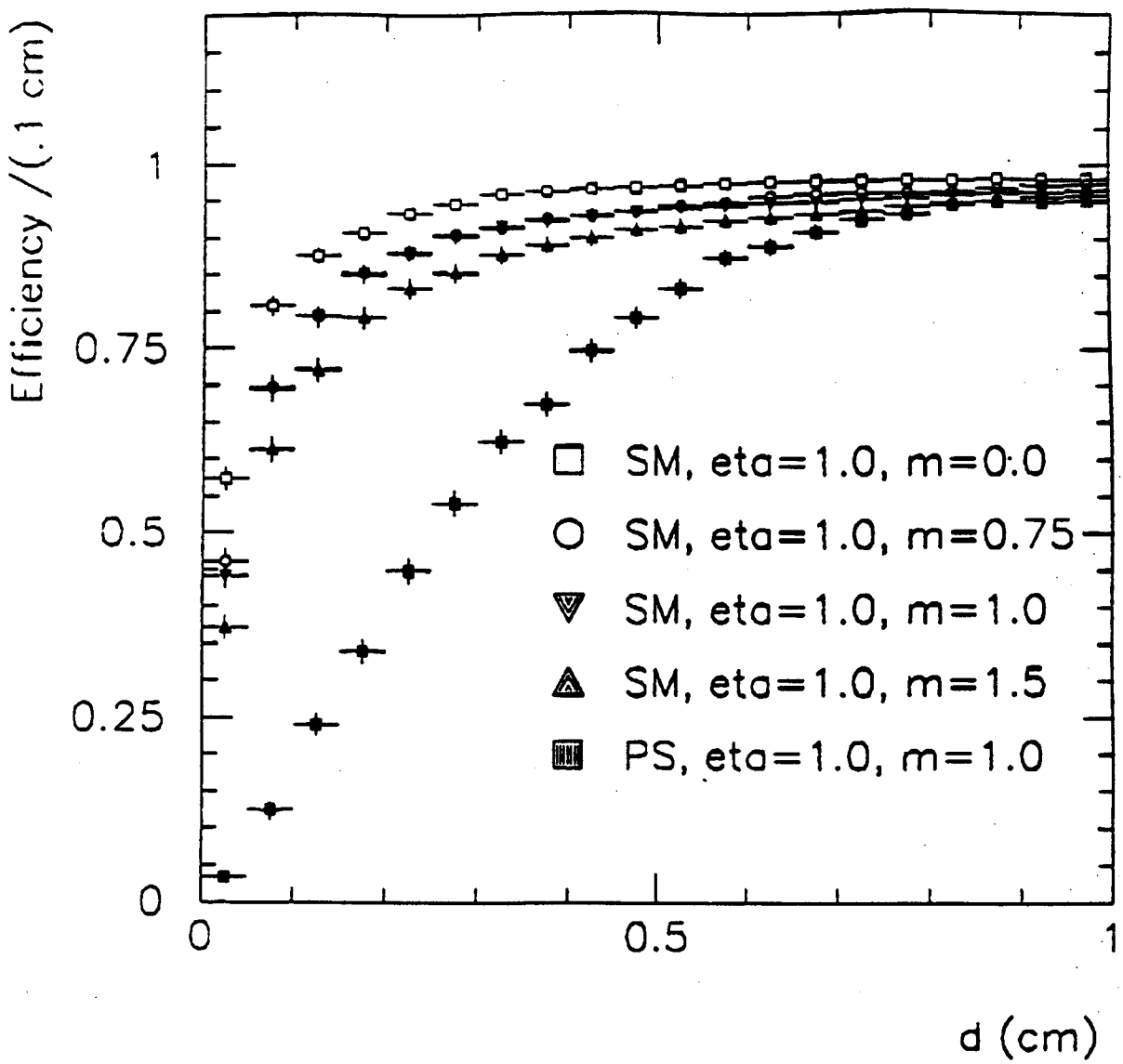

Figure 16: Efficiency of finding a shower inside of a rectangle with dimension d in the non-bend plane and $2d$ in the bend plane as a function of d for different amount of tracking materials at $\eta = 1.0$

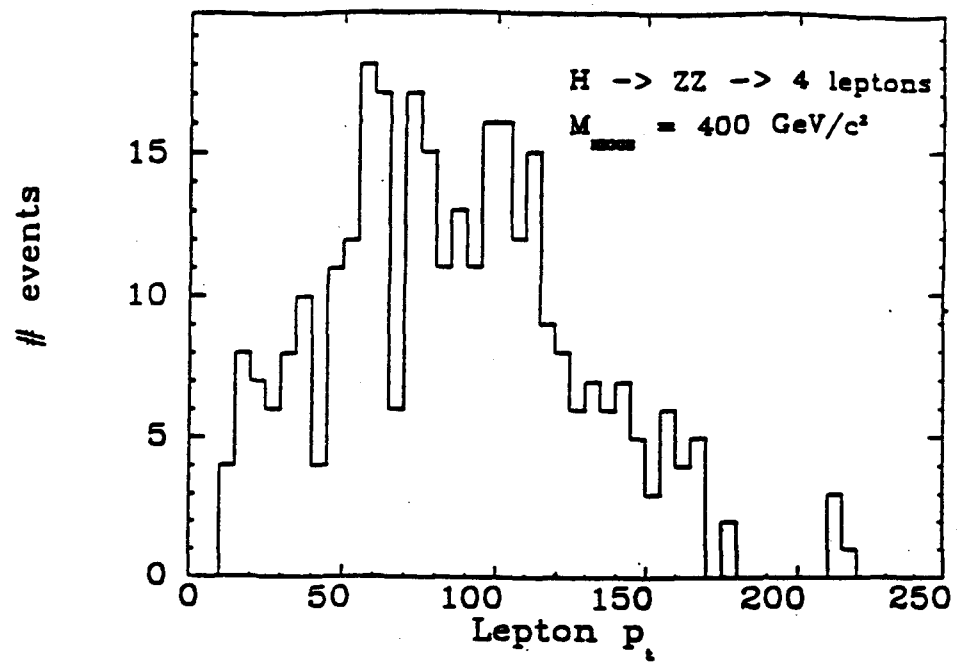

Figure 17:Lepton p_t distribution from Isajet for a 400 GeV/c^2 Higgs boson

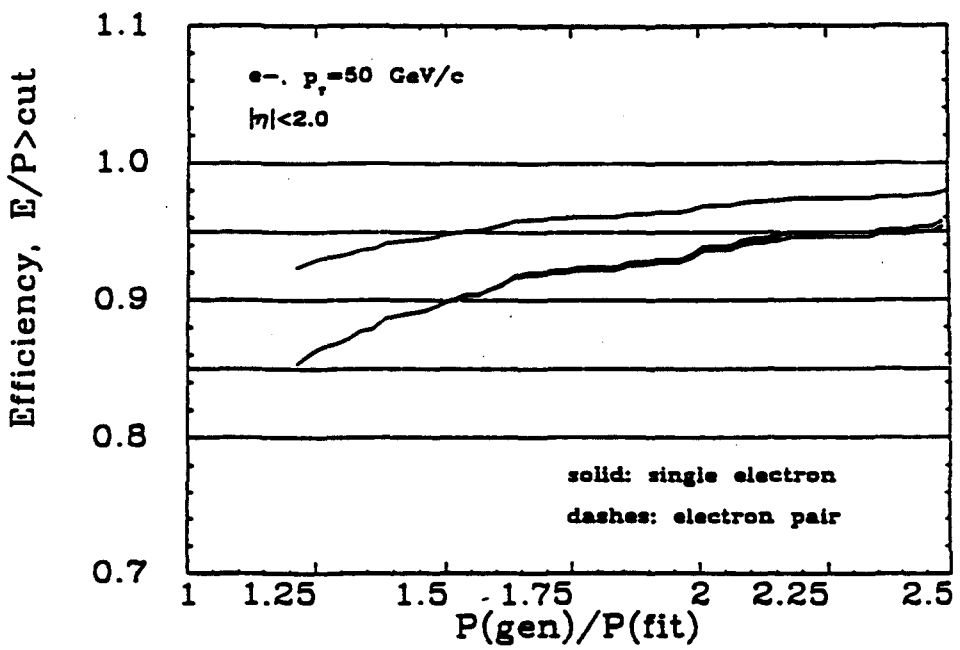

Figure 18:E/p efficiency for a pair of electrons compared with the single electron efficiency. For the pair efficiency, two curves show the efficiency for symmetric cuts in E/p and a tight cut ($E/p < 1.2$) for one electron vs the looser E/p cut applied to the other.

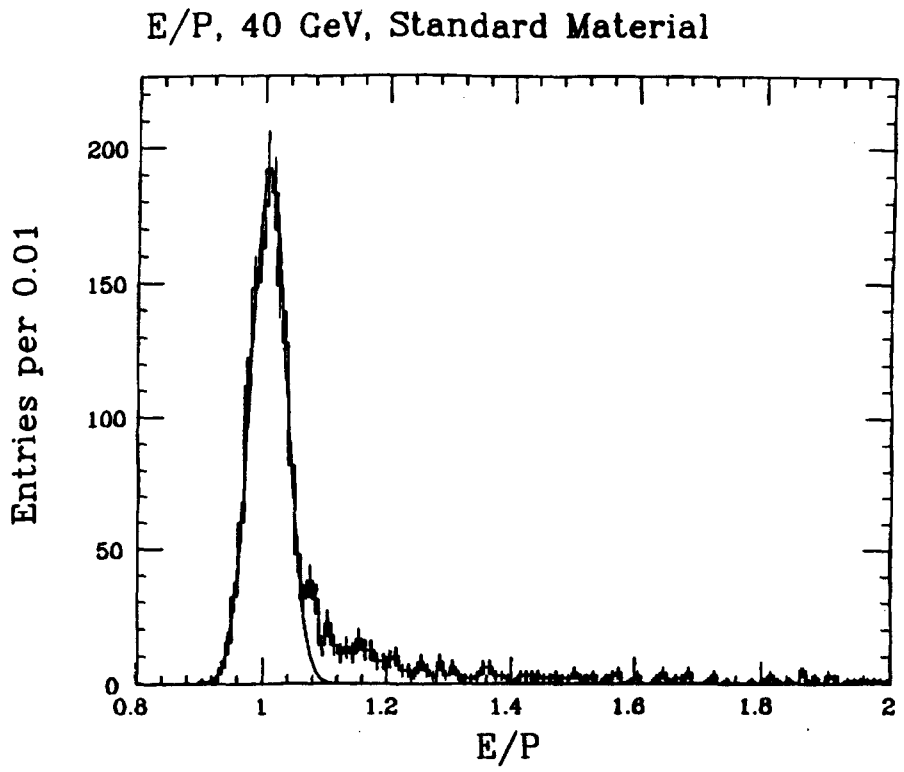

Fig. 19a

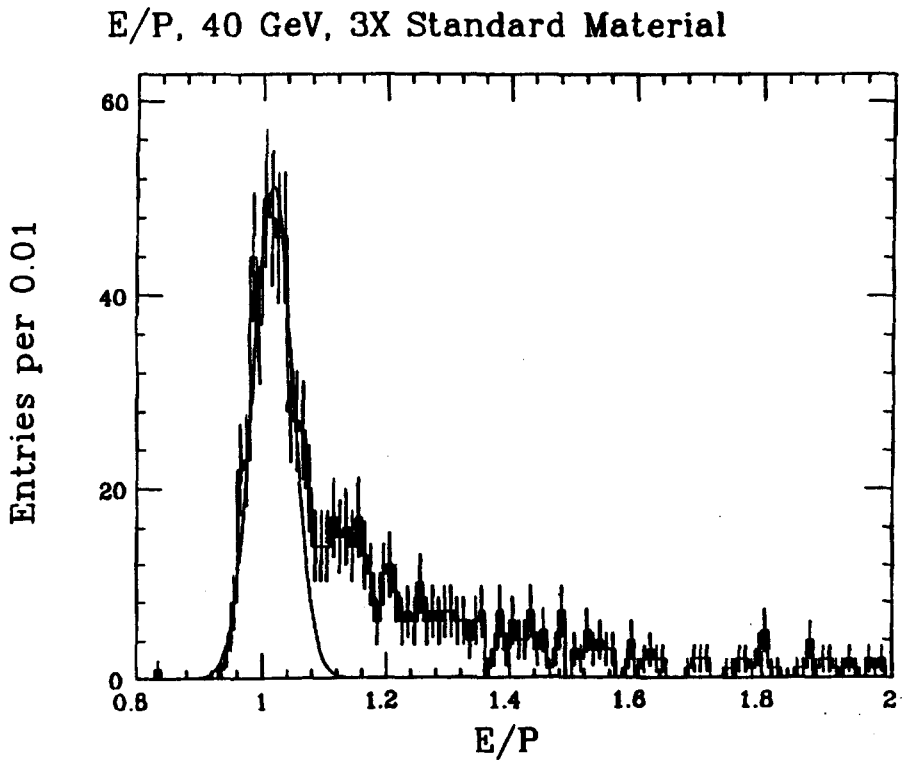

Fig 19b

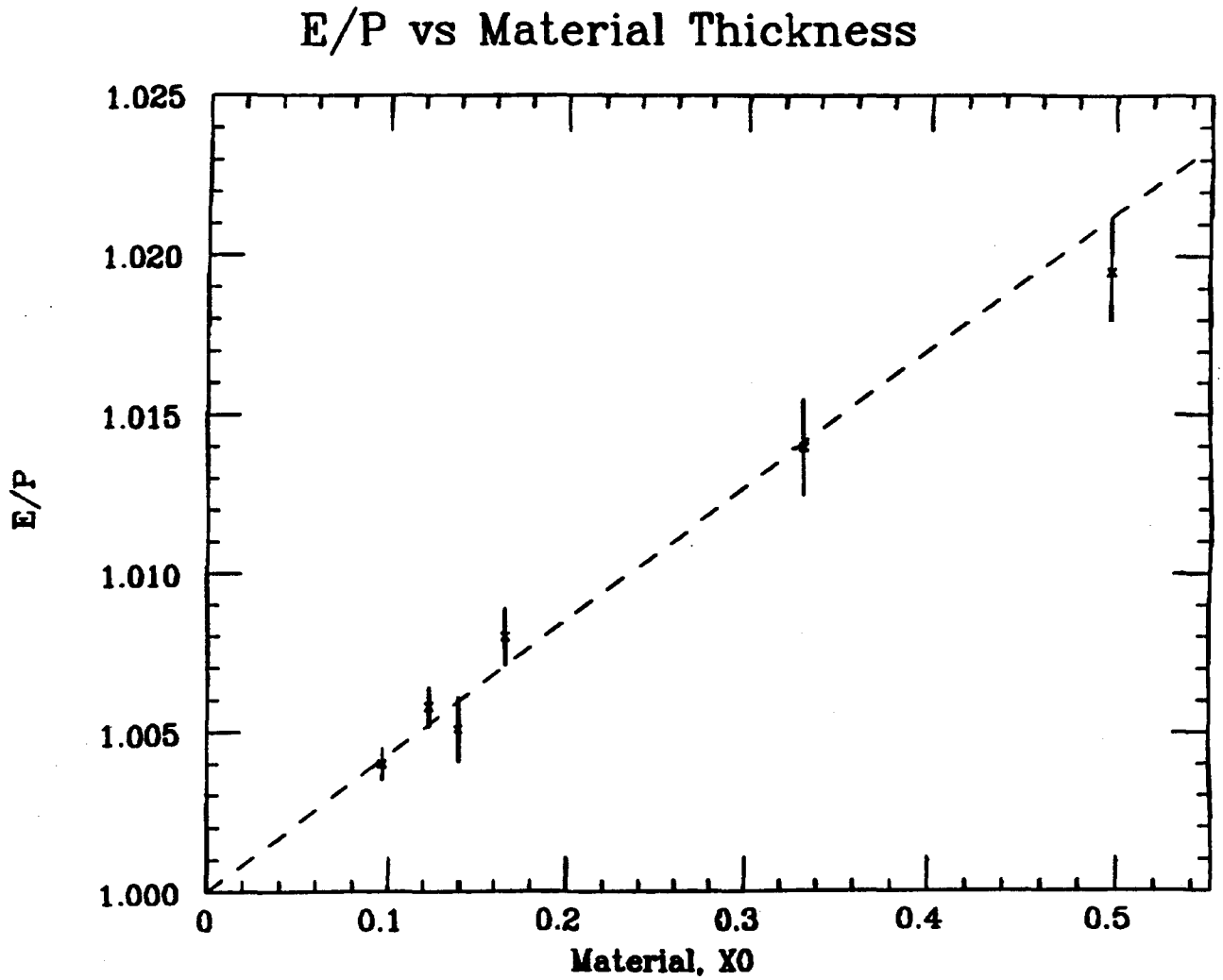
E/P vs Material Thickness
1.025
1.020
1.015
1.010
1.005
1.000
E/P
0
0.1
0.2
0.3
0.4
0.5
Material, X0

Fig.20

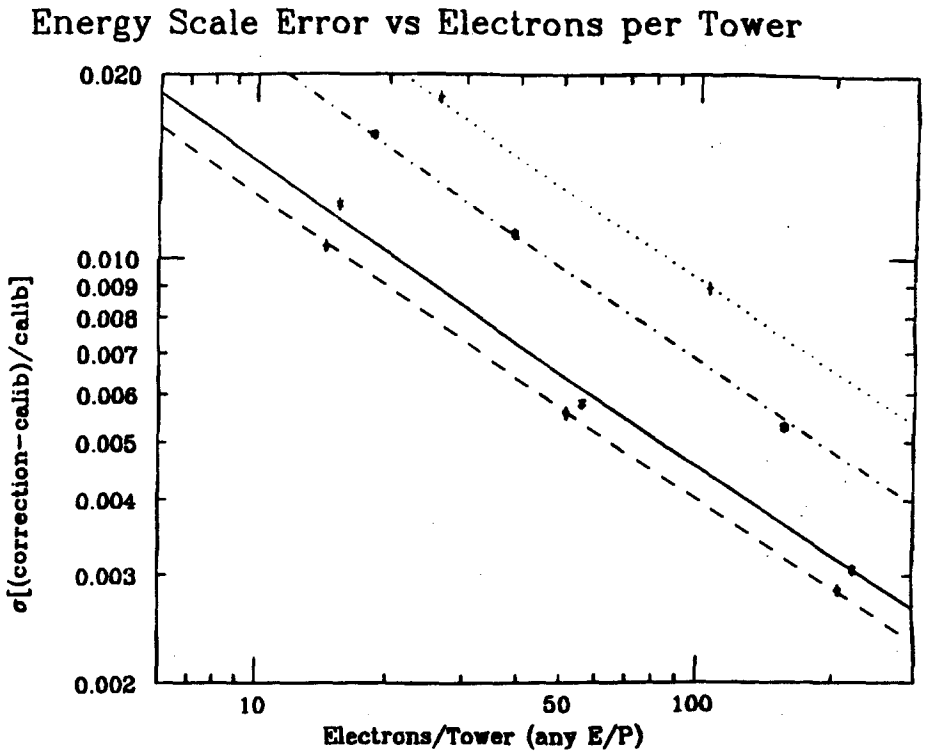
Energy Scale Error vs Electrons per Tower
0.020
0.010
0.009
0.008
0.007
0.006
0.005
0.004
0.003
0.002
σ[(correction−calib)/calib]
10
50
100
Electrons/Tower (any E/P)

Fig. 21

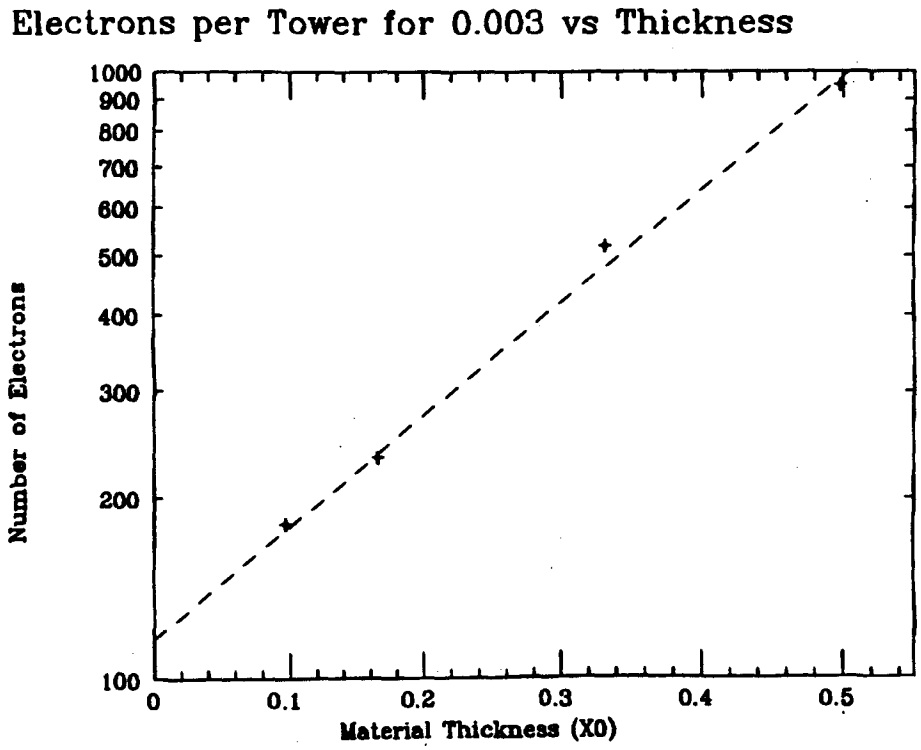
Electrons per Tower for 0.003 vs Thickness
1000
900
800
700
600
500
400
300
200
100
Number of Electrons
0
0.1
0.2
0.3
0.4
0.5
Material Thickness (X0)

Fig. 22

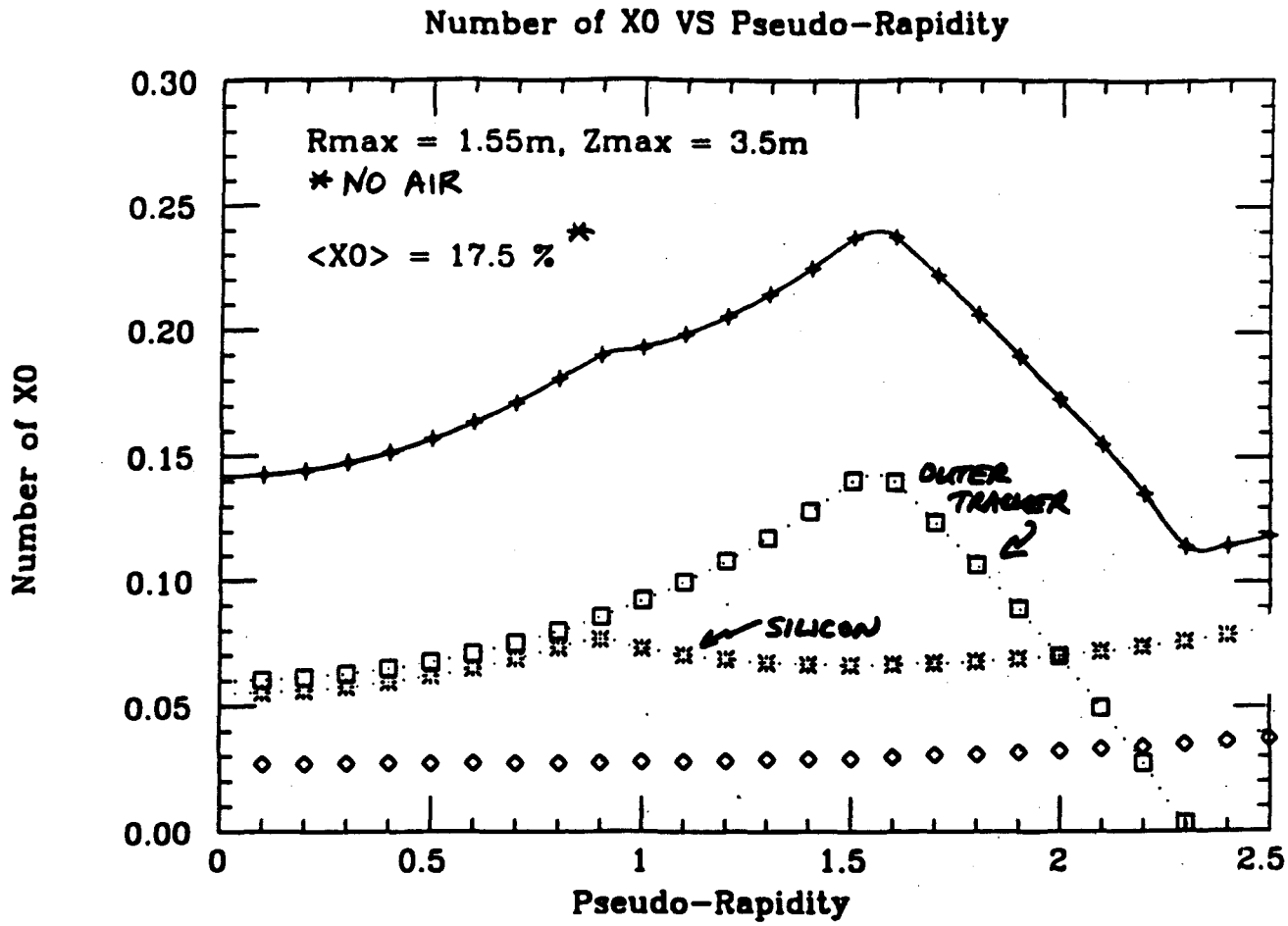
Number of X0 VS Pseudo-Rapidity
Rmax = 1.55m, Zmax = 3.5m
* NO AIR
<X0> = 17.5 % *
OUTER TRACKER
SILICON
Number of X0
Pseudo-Rapidity
0.30
0.25
0.20
0.15
0.10
0.05
0.00
0
0.5
1
1.5
2
2.5

Fig 23